Distinct Roles of Cyclones and Anticyclones in Setting the Midwinter Minimum of the North Pacific Eddy Activity: A Lagrangian Perspective

SATORU OKAJIMA,[a] HISASHI NAKAMURA,[a] AND YOHAI KASPI[b]

[a] *Research Center for Advanced Science and Technology, The University of Tokyo, Tokyo, Japan*
[b] *Department of Earth and Planetary Sciences, Weizmann Institute of Science, Rehovot, Israel*

(Manuscript received 26 June 2022, in final form 14 March 2023, accepted 20 March 2023)

ABSTRACT: The North Pacific storm-track activity is suppressed substantially under the excessively strong westerlies to form a distinct minimum in midwinter, which seems inconsistent with linear baroclinic instability theory. This "midwinter minimum" of the storm-track activity has been intensively investigated for decades as a test case for storm-track dynamics. However, the mechanisms controlling it are yet to be fully unveiled and are still under debate. Here we investigate the detailed seasonal evolution of the climatological density of surface migratory anticyclones over the North Pacific, in comparison with its counterpart for cyclones, based on a Lagrangian tracking algorithm. We demonstrate that the frequency of surface cyclones over the North Pacific maximizes in midwinter, whereas that of anticyclones exhibits a distinct midwinter minimum under the upstream influence, especially from the Japan Sea region. In midwinter, it is only on such a rare occasion that prominent weakening of the East Asian winter monsoon allows a migratory surface anticyclone to form over the Japan Sea, despite the unfavorable climatological-mean conditions due to persistent monsoonal cold-air outbreaks and the excessively strong upper-tropospheric westerlies. The midwinter minimum of the North Pacific anticyclone density suggests that anticyclones are likely the key to understanding the midwinter minimum of the North Pacific storm-track activity as measured by Eulerian eddy statistics.

KEYWORDS: Asia; North Pacific Ocean; Anticyclones; Storm tracks; Decadal variability; Seasonal cycle

1. Introduction

In midlatitudes, transient cyclones and anticyclones successively develop in traveling eastward, leaving stacks of their tracks, often called "storm tracks." Those transient disturbances do not merely regulate day-to-day weather variations in the extratropics, but also interact with a background state to maintain the climatological-mean state such as the distinct midlatitude westerly jets, and the global atmospheric energy budget through transporting momentum and heat systematically.

Studies of such subweekly transient disturbances have arisen from the surveillance of the path and intensity of "storms." In the late nineteenth century, typical paths of storms were recognized reasonably in the Euro-Atlantic sector (Hinman 1888). Until the late twentieth century, distribution of cyclone frequency has been examined based on surface weather charts (Klein 1958; Whittaker and Horn 1984) to reveal that cyclone frequency is particularly high over the North Pacific (NP) and North Atlantic (NA). With the development of atmospheric gridded data, procedures have been proposed to identify centers of cyclones and anticyclones more objectively (e.g., Parker et al. 1989; Bell and Bosart 1989; Murray and Simmonds 1991; Hodges 1994, 1995). Until today, many studies have utilized various tracking algorithms (Ulbrich et al. 2009; Neu et al. 2013). They identify and track centers of cyclones or anticyclones based typically on fields of sea level pressure (SLP) or low-level vorticity. These "Lagrangian" tracking algorithms enable us to analyze individual transient eddies and associated phenomena, including winds, temperature, and precipitation. Based on identified low-level cyclonic centers, composited structures of cyclones have been constructed by using atmospheric reanalysis data (Manobianco 1989; Wang and Rogers 2001) and output of a general circulation model (GCM) experiment (Catto et al. 2010).

The development of another methodology for storm-track studies based on an "Eulerian" perspective lagged behind the Lagrangian method. Pioneering works such as Sawyer (1970) and Blackmon (1976) suggested that regions of particularly large bandpass-filtered fluctuations of 500-hPa height closely correspond to those of frequent cyclone paths over the NA and NP basins. Since then, (co)variance of bandpass- or high-pass-filtered fluctuations has been commonly used as a local measure of activity of extratropical transient eddies (e.g., Blackmon et al. 1977, 1984; Chang et al. 2002; Nakamura et al. 2004).

According to the theory of baroclinic instability, stronger vertical shear of the westerlies is equivalent to larger maximum growth rate of eddies (Eady 1949). Consistently with this principle, the NA storm-track activity is on average maximized in midwinter, when the climatological-mean upper-tropospheric westerly jet speed peaks. The corresponding NP storm-track activity, to the contrary, exhibits a distinct minimum in midwinter despite the maximum speed of the

Denotes content that is immediately available upon publication as open access.

Supplemental information related to this paper is available at the Journals Online website: https://doi.org/10.1175/JCLI-D-22-0474.s1.

Corresponding author: Satoru Okajima, okajima@atmos.rcast.u-tokyo.ac.jp

DOI: 10.1175/JCLI-D-22-0474.1

upper-tropospheric westerly jet (Nakamura 1992), which is apparently inconsistent with the baroclinic instability theory.

This distinctive seasonality is referred to as "midwinter minimum" (MWM) or "midwinter suppression" of the NP storm-track activity. It has long been investigated from various viewpoints as a "test case" for the midlatitude storm-track dynamics. The MWM of the NP storm track is also simulated in numerical models. Zhang and Held (1999) successfully simulated the MWM in a stochastic linear storm-track model, implying that it is mainly caused by linear dry dynamics. In contrast, a similar effort by Whitaker and Sardeshmukh (1998) was unsuccessful. Chang and Zurita-Gotor (2007) were also unsuccessful in simulating the MWM with an idealized nonlinear storm-track model. The MWM is represented in a GCM (Christoph et al. 1997), and it is generally reproduced in the historical experiment with CMIP6 GCMs (Yang et al. 2021). Furthermore, Martian reanalysis datasets reveal transient eddy activity exhibits a minimum around winter solstice (*solstitial pause*; Lewis et al. 2016; Battalio 2022).

Since its discovery, multiple mechanisms have been proposed for the explanation of the MWM of the NP storm-track activity. Harnik and Chang (2004) as well as Deng and Mak (2005) pointed out the possible influence of the prominent lateral shear of the excessively strong midwinter jet on the suppressed growth rate of baroclinic eddies through the "barotropic governor" effect, which is related to the results obtained by James (1987). As for the jet structure, the seasonal transition of the NP jet characteristics between stronger and more subtropical "merged" jet in midwinter and weaker eddy-driven "separate" jet in the shoulder seasons may be responsible for the MWM of the storm-track activity (Lachmy and Harnik 2014, 2016; Yuval et al. 2018; Yuval and Kaspi 2018). Using an idealized GCM with zonally symmetric settings, Novak et al. (2020) emphasized the importance of the climatological southward shift of the Pacific jet in midwinter. As supportive evidence for the importance of the jet intensity, Afargan and Kaspi (2017) found a clear suppression of high-frequency eddy activity even over the NA in cases of the particularly strong NA jet in midwinter. Those cases were also characterized by the jet being anomalously equatorward. Nakamura (1992) and Nakamura et al. (2002) suggested that the baroclinic development of transient eddies may be inhibited under their excessive propagation speed owing to shortening the residence time over the baroclinic zone. Nakamura and Sampe (2002) pointed out that upper-level eddies tend to be trapped into the equatorward- and upward-shifted "hybrid" NP jet core in midwinter and are therefore more likely to be disconnected from the near-surface baroclinic zone, which is thus unfavorable for effective baroclinic growth of eddies. In addition, the effect of diabatic heating associated with low-level clouds in the cold sector of surface cyclones was investigated by Chang (2001) and Chang and Song (2006). Park et al. (2010) and Lee et al. (2013) suggested the potential importance of large-scale orography.

Instead of taking a process-by-process approach, some studies have taken advantage of a framework of atmospheric energetics (Chang 2001; Zhao and Liang 2019; Schemm and Rivière 2019), which has evolved in the framework put forward by Lorenz (1955). Most recently, Okajima et al. (2022) evaluated the detailed seasonal evolution of energy conversion/generation rates associated with transient eddies along the NP storm track, in a normalized fashion by the eddy total energy. Their energetics was performed from a comprehensive perspective of the MWM of the NP storm-track activity that encompasses various mechanisms proposed by previous studies. They pointed out that the net normalized energy conversion/generation rate is indeed suppressed in midwinter. Specifically, eddy available potential energy conversion plays a substantial role especially in the reduction of the net normalized energy conversion/generation rate from its early winter peak, whereas that of the net energy influx into the NP is of particular importance for the spring recovery.

The above studies are based basically on Eulerian eddy statistics. Studies of the MWM of the NP storm-track activity from the Lagrangian perspective have been relatively few. Penny et al. (2010) focused on the importance of upper-level cyclonic eddies propagating from the Asian continent upstream of the storm track ("seeding effect"), through a Lagrangian tracking method. They suggested that a significant seasonal reduction of cyclonic eddies is responsible for the MWM, although no such clear relationship was found in an independent analysis by Chang and Guo (2012). Hoskins and Hodges (2019a,b) investigated seasonal evolution of the number and intensity of meridional wind maxima over the Northern Hemisphere. They demonstrated that, in the western NP, both the number and intensity of upper-tropospheric eddies along the storm-track axis tend to minimize in midwinter, while the number of lower-tropospheric eddies peaks in midwinter but their intensity exhibits a weak MWM. Schemm and Schneider (2018) examined the relationship among storm-track activity, number, and lifetime of surface cyclones over the NP. They suggested that shorter lifetime of cyclones in midwinter may contribute to the MWM of the Eulerian storm-track activity. Subsequently, Schemm et al. (2021) suggested that cyclones downstream of Kamchatka are less numerous and less intense in January, contributing primarily to the MWM of the NP storm-track activity, along with a contribution from cyclones moving from the East China Sea (ECS) to the spring recovery of the NP storm-track activity. Most recently, through tracking of upper- and lower-tropospheric cyclonic eddies in idealized GCM simulations in which the jet strength was systematically increased, Hadas and Kaspi (2021) investigated the dependence of the number, intensity, and lifetime of those eddies on the jet intensity. As the jet strengthens and the corresponding vertical shear increases in the model, they found clear tendencies that their coupling between the upper and lower levels diminishes, their westward-tilting baroclinic structure becomes broken and thus their baroclinic growth becomes suppressed. These tendencies can therefore result in an inverse relation between jet intensity and eddy growth under the excessively strong jet.

One of the major difficulties in understanding the MWM is a gap between the "Lagrangian" statistics of moving cyclones and "Eulerian" eddy statistics that depict the MWM of the NP storm-track activity. The latter regards transient eddies as waves where contributions from both cyclonic and anticyclonic

deviations are combined (Wallace et al. 1988). Meanwhile, those studies of the MWM from the Lagrangian perspective focus mainly on cyclones, while excluding the potential contribution from anticyclones, which makes it difficult to compare quantitatively the results obtained from the two different perspectives. Of course, there is no necessity for measures of eddy activity from the Lagrangian and Eulerian perspectives to accord with one another. In Schemm and Schneider (2018), for instance, distributions of Lagrangian surface cyclone density and Eulerian eddy activity differ substantially over the NP; the former is highest over the Gulf of Alaska, whereas the latter maximizes along a zonal band at ~40°N. A similar difference is also shown by Shaw et al. (2016).

With more attention paid to extratropical cyclones that are directly related to stormy weather, few studies have focused on the climatological-mean behavior of migratory anticyclones based on a tracking, especially over the NP. Hoskins and Hodges (2002) found that climatological wintertime distributions of cyclone and anticyclone densities distinctively differ over the NP. Specifically, the former is highest to the east of Japan, while the latter peaks along ~30°N. Since then, some studies have conducted a feature-tracking analysis for migratory anticyclones over the NP (Favre and Gershunov 2006; Ioannidou and Yau 2008; Kravtsov et al. 2015; Pepler et al. 2019), but they did not focus on the relationship between anticyclone tracks and storm-track activity measured as Eulerian eddy statistics. All in all, the role of migratory anticyclones in the formation and seasonality of the "NP storm track" within the Eulerian framework is still not well understood.

Recently, Okajima et al. (2021, hereafter cited as ONK21) have developed a method to separate cyclonic and anticyclonic contributions to Eulerian eddy statistics. They revealed that anticyclonic vortices play an important role in maintaining the midwinter Pacific jet, especially in the upper troposphere, and they make greater contributions to the barotropic energy conversion and net energy outflow for the midwinter NP storm track. Their results therefore suggest that anticyclones should not be dismissed in investigating the MWM of the NP storm track from the Lagrangian perspective.

To this end, the present study aims at investigating the detailed seasonal evolution of climatological density of surface migratory anticyclones over the NP, in comparison with its counterpart of cyclones, based on a Lagrangian tracking algorithm. We demonstrate that the seasonality of the frequency of surface anticyclones is substantially contributed by the upstream influence from the Japan Sea region and thus differs distinctively from that of cyclones.

This paper is organized as follows: Section 2 explains data and analysis methods used in this study. Section 3 describes seasonal evolution of climatological-mean activity of NP cyclones and anticyclones. Then, composite analysis is conducted to investigate mechanisms for the seasonality in section 4. Section 5 examines long-term modulations of the densities of cyclone and anticyclone centers. Section 6 offers a summary and discussion.

2. Data and analysis methods

a. Observational data

This study utilizes 6-hourly fields of atmospheric variables, including geopotential height, temperature, and wind velocities in pressure coordinates as well as sea level pressure (SLP), taken from the Japanese 55-year Reanalysis (JRA-55) by the Japan Meteorological Agency (JMA) (Kobayashi et al. 2015; Harada et al. 2016) for the period 1958–2017. The JRA-55 has been constructed with a four-dimensional variational data assimilation (4D-Var) system with TL319 horizontal resolution (equivalent to 55-km resolution) and 60 vertical level up to the 0.1-hPa level. Those variables are available on a 1.25° × 1.25° grid.

At each grid point, subweekly fluctuations associated with synoptic-scale transient eddies have been extracted from the 6-hourly atmospheric reanalysis through an 8-day cutoff Lanczos filter with a 121-point window. Their low-frequency modulations have then been calculated locally as low-pass-filtered fields of their products, to represent eddy activity of fluxes. Climatological-mean fields are calculated with a 31-day running mean. A composited map is created for each calendar days from 59 years of data and then 31-day running mean is applied to it unless noted otherwise.

b. Identification of tracks of surface migratory cyclones and anticyclones

In this study, tracks of migratory cyclones and anticyclones are objectively identified based on the total SLP of the JRA-55 dataset, by identifying cyclones and anticyclones on a surface weather map, taking the different typical characteristics of cyclones and anticyclones into account. This means that in this study cyclones and anticyclones are identified as systems having their own structures, which interact with and include the influence from low-frequency variabilities and climatological background states. Tracking with the total SLP has been also carried out by other recent studies focusing on the Lagrangian perspective of the MWM of the NP storm-track activity (e.g., Schemm et al. 2021). Assessment of the performance of the tracking algorithm is thus provided in the appendix. We have also confirmed the robustness of tracking results with ~6000-yr output of a large-ensemble GCM experiment (online supplementary Figs. S1 and S2).

1) CYCLONE TRACKS

For identifying surface cyclone centers, we adopt a tracking algorithm used by Kuwano-Yoshida et al. (2022). SLP and its Laplacian (hereafter ∇^2SLP) are utilized to identify cyclones on a surface weather map. The combination of SLP and ∇^2SLP (or surface vorticity) has been adopted to identify cyclone tracks in previous studies (e.g., Murray and Simmonds 1991; Pinto et al. 2005; Simmonds et al. 2008; Hewson and Titley 2010). Before initiating the tracking, a Gaussian spatial filter whose half-amplitude length is 300 km was applied to ∇^2SLP to obtain a smoother field. Those grid points at which surface elevations are higher than 1500 m were not used for the tracking to avoid identifying spurious centers.

First, local minima of SLP were regarded as candidates for cyclone centers, and among them only the SLP minimum with the lowest pressure in the vicinity of a 400-km circle has been identified. The SLP minimum must accompany a local maximum of ∇^2SLP within 700 km, which must be stronger than 80 Pa (100 km)$^{-2}$. This condition was imposed to discard weak cyclones with no significant amplitudes.

Next, those SLP minima identified above were compiled as tracks. Specifically, the nearest SLP minima at successive time steps were connected, only when their distance is not more than 800 km. Any track must persist at least over four time steps (viz., 24 h) and must travel at least over 600 km during the lifetime.[1] A cyclone track must pass through a domain encompassing the NP storm track (20°–65°N, 100°E–120°W).

2) ANTICYCLONE TRACKS

For anticyclones, only SLP was used to identify their centers as in previous studies (Hoskins and Hodges 2002; Kravtsov et al. 2015). Unlike cyclones, anticyclones are unlikely to have distinct ∇^2SLP minima, reflecting the gradient wind balance. Local SLP maxima were regarded as candidates for anticyclone centers, after SLP has been horizontally smoothed with performing a nine-point horizontal smoothing (weight is 0.5 next to the center point and 0.3 at corners) eight times. Here, only an SLP maximum that is highest within a 400 -km circle around the maximum was identified as a surface anticyclonic center at which SLP should not be lower than 990 hPa.

Similar to the case for cyclone centers, the nearest SLP maxima identified above at successive time steps were connected. The distance must not exceed 1000 km. Again, any track must persist at least over four time steps (i.e., 24 h) and travel at least over 600 km during the lifetime. The distribution of their density is similar if longer thresholds for movement are imposed. Any anticyclone track must pass through the domain (20°–65°N, 100°E–120°W) around the NP storm track.

3. Climatological-mean activity of North Pacific cyclones and anticyclones

Figure 1 shows horizontal distributions of climatological-mean densities of cyclone and anticyclone centers[2] from November to March. As shown in previous studies, the cyclone density is high over the NP poleward of 30°–35°N, in association with the climatological-mean Aleutian low (AL). Those cyclones tend to move eastward or northeastward (not shown; e.g., Tamarin and Kaspi 2016). Around the climatological-mean AL center, density of migratory cyclones maximizes in midwinter (Fig. 1c). Just off the east coast of Japan at ~35°N, a hint of a local maximum of the cyclone density suggests the influence from the warm Kuroshio Extension (KE) on the development of synoptic- and meso-α-scale cyclones (Masunaga et al. 2020), especially from midwinter to early spring. Another noticeable feature is high density along the south coast of Japan in spring (Figs. 1d,e), corresponding to frequent "southern coast cyclones" around Japan (Takano 2002).

In contrast, the anticyclone density exhibits a zonally extended band of maxima at ~30°N, slightly poleward of the climatological-mean subtropical high pressure belt. The contrasting latitudes of the density maxima of cyclones and anticyclones are consistent with Hoskins and Hodges (2002). Migratory anticyclones over the western and central NP tend to move eastward or slightly southeastward especially in midwinter (not shown). The different moving directions between cyclones and anticyclones are consistent with previous studies (Wallace et al. 1988; Tamarin and Kaspi 2016). The maximum over the eastern NP collocates with the climatological-mean center of the subtropical high (Nakamura et al. 2010). The zonally elongated band of the high density is consistent with Pepler et al. (2019, their Fig. 2), though the eastern NP maximum is somewhat more emphasized in this study, which is discussed in the appendix. The density is also high over the Yellow Sea in addition to eastern and northern China, which may correspond to synoptic-scale anticyclones that are separated from the persistent Siberian high. The anticyclone density in the storm-track entrance region (at ~40°N, 140°E) is reduced in midwinter compared with that in the shoulder seasons.

To highlight the seasonality of the cyclonic and anticyclonic densities in the NP storm-track core region, their latitude–season sections as zonal means for 150°E–160°W are shown in Fig. 2. Cyclone density maximizes in midwinter, coinciding with the climatological peak of the AL (Fig. 2a). The seasonality of the cyclone density in Fig. 2 is consistent with the seasonality of the cyclone number found by Schemm and Schneider (2018). The region of highest cyclone density extends most southward in midwinter, leading to its striking midwinter maximum between 40° and 50°N. Identified cyclones tend to propagate at a speed corresponding to the climatological-mean U_{700} (~12 m s^{-1} at the density maximum), although their typical movement is relatively slow (<~6 m s^{-1}) north of ~50°N in midwinter (Fig. 2a), contributing partly to the high-density there under the influence of the quasi-stationary AL. Meanwhile, the latitude of maximum anticyclonic density migrates southward from 35° to °43°N in the shoulder seasons to ~30°N in midwinter along with the subtropical high pressure belt (Fig. 2b). They tend to travel at a speed corresponding to the climatological-mean U_{700} (>12 m s^{-1}) along the axis of their density maximum (Fig. 2b). In sharp contrast to the cyclonic density, the anticyclonic density shows its distinct MWM. The regions of frequent cyclones and anticyclones are roughly separated by the lower-tropospheric westerly jet axis.

[1] The seasonal evolution of the climatological-mean densities of cyclones and anticyclones is qualitatively the same with a minimum traveling distance of 1000 km.

[2] Hereafter, density is defined as the occurrence of time steps when a cyclone/anticyclone center exists at each grid point divided by the number of total time steps. We are aware that density of those centers is affected by both the number of tracks and their lifetime. The present study focuses on density, because it can be compared with Eulerian eddy statistics in a more straightforward manner than the number of tracks, as well as it bypassing the potential uncertainty owing to splitting of tracks. Nevertheless, the influence of the number and duration is discussed in section 6.

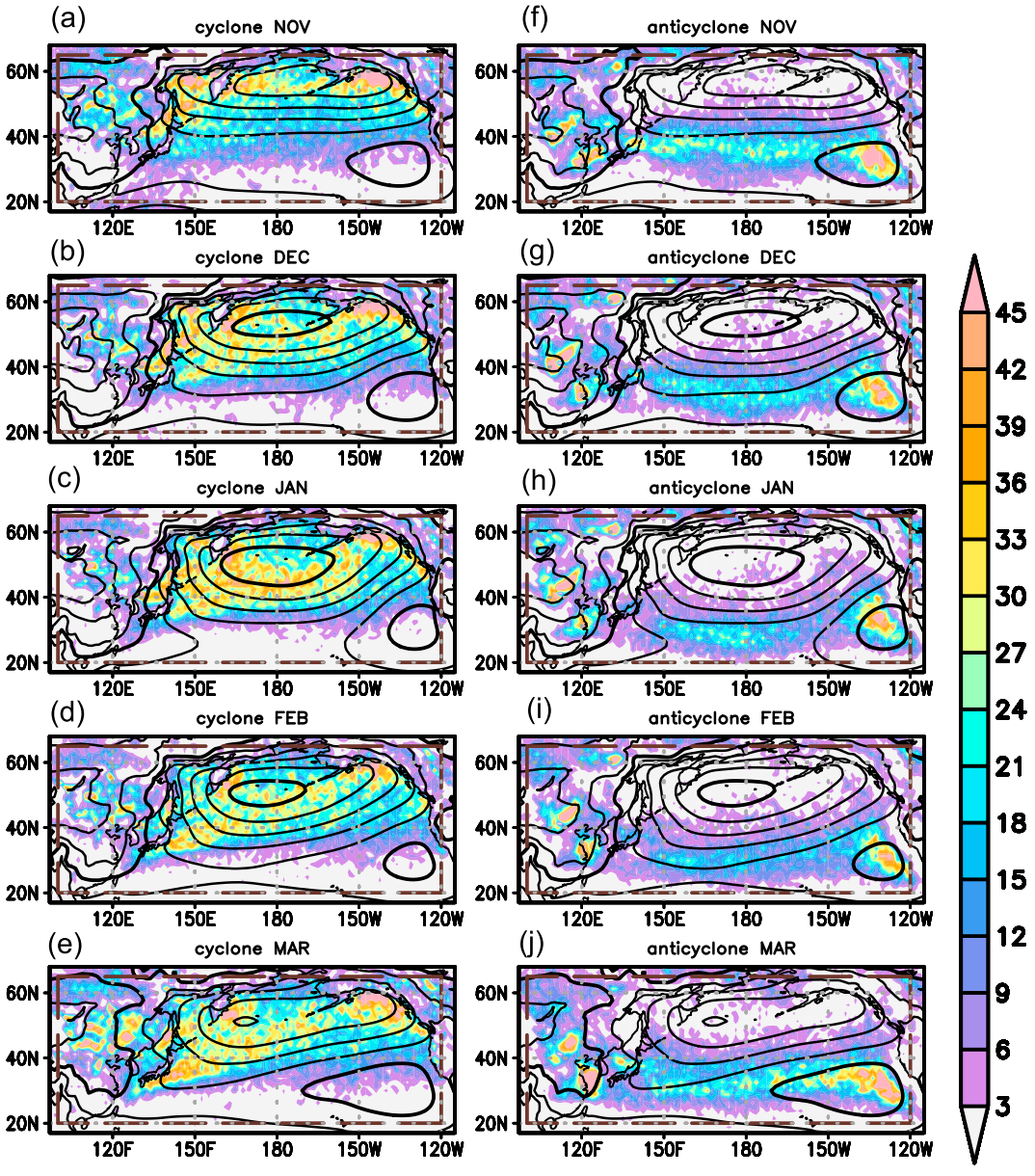

FIG. 1. Climatological-mean densities (×0.01%) of identified surface (a)–(e) cyclone and (f)–(j) anticyclone centers for the calendar months as indicated, based on 6-hourly SLP fields of the JRA-55 for the period 1958/59–2016/17. Meridians of 100°E and 120°W, and latitude circles of 20° and 65°N are highlighted, which indicate the lateral boundaries of the domain through which those centers must pass. Contours indicate climatological-mean SLP (every 4 hPa, thick for every 20 hPa).

The contrasting seasonality between surface cyclone and anticyclone densities has not been described in previous studies. One may consider that the midwinter maximum of cyclone density may be compatible with the stronger westerly jet and baroclinicity in midwinter than in the shoulder seasons, leading to higher maximum growth rate of baroclinic eddies, which may also influence their intensity and lifetime. At the same time, however, the seasonality of the NP cyclone density suggests that it may not be responsible for the MWM of the NP storm-track activity as measured by Eulerian statistics. As another factor contributing to the seasonality in Eulerian eddy statistics, Hoskins and Hodges (2019b) showed that eddy amplitude (measured by the magnitude of tracked local maxima of positive or negative meridional wind speed) is reduced in midwinter. The seasonality in the cyclone intensity evaluated by the magnitude of spatially smoothed ∇^2SLP maxima corresponding to identified cyclone centers also exhibits a moderate MWM (10%–15%; not shown), but it may be overwhelmed by the midwinter increase in the number of cyclones as shown in Fig. 2a. The contrasting seasonality

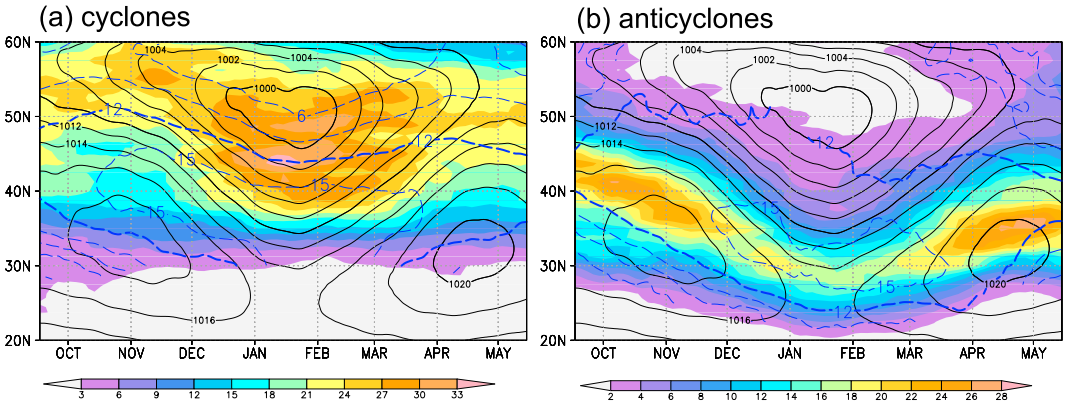

FIG. 2. Latitude–season sections of climatological-mean densities (×0.01%) of surface (a) cyclone and (b) anticyclone centers identified over the central NP based on 6-hourly SLP fields of the JRA-55 for the period 1958/59–2016/17. Black contours indicate climatological-mean SLP (every 2 hPa, thickened for every 10 hPa). Blue dashed contours signify the climatological-mean scalar moving speed (every 3 m s^{-1}, thickened for 12 m s^{-1}) of identified centers. The climatological-mean propagation speeds are weakly smoothed meridionally before plotted except for domains where their climatological-mean densities are low (less than 0.03% and 0.02%, respectively). All the quantities are longitudinally averaged between 150°E and 160°W. Labels on the abscissa mark the beginnings of the individual calendar months.

suggests that migratory anticyclones can be of certain importance for the MWM of the NP storm-track activity.

To delineate the striking difference in the seasonality between cyclone and anticyclone densities, only tracks passing the central NP domain (20°–65°N, 150°E–150°W) are counted to illustrate where cyclones and anticyclones detected within the storm-track core region come from. The three calendar days in Fig. 3 correspond to the first peak, MWM, and the second peak of the NP storm-track activity during its seasonal cycle, based on lower-tropospheric Eulerian eddy statistics (Okajima et al. 2022). The NP cyclones tend to propagate from the northern Japan Sea and the Okhotsk Sea in early winter (Fig. 3a), whereas in spring more cyclones tend to travel along the Kuroshio just south of Japan and then along the KE (Fig. 3c). Propagation

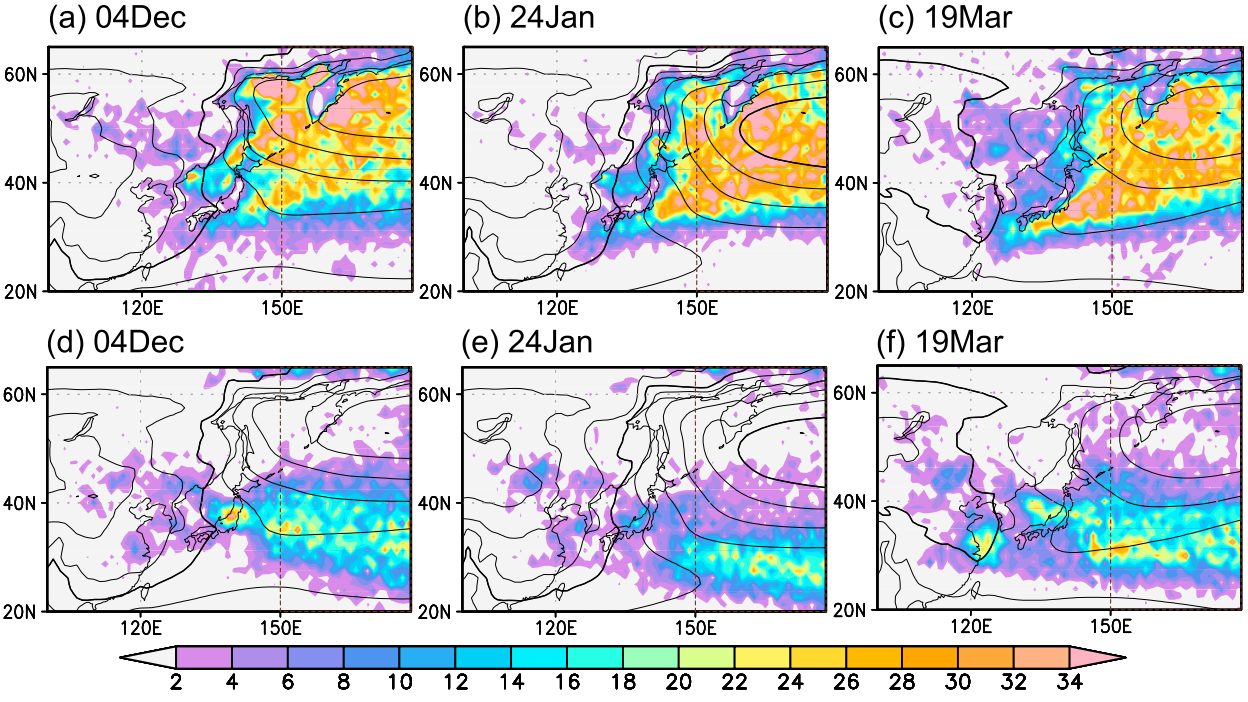

FIG. 3. As in Fig. 1, but for identified surface (a)–(c) cyclone and (d)–(f) anticyclone centers passing through the domain of 20°–65°N, 150°E–150°W over the central NP as climatologies for the calendar days as indicated.

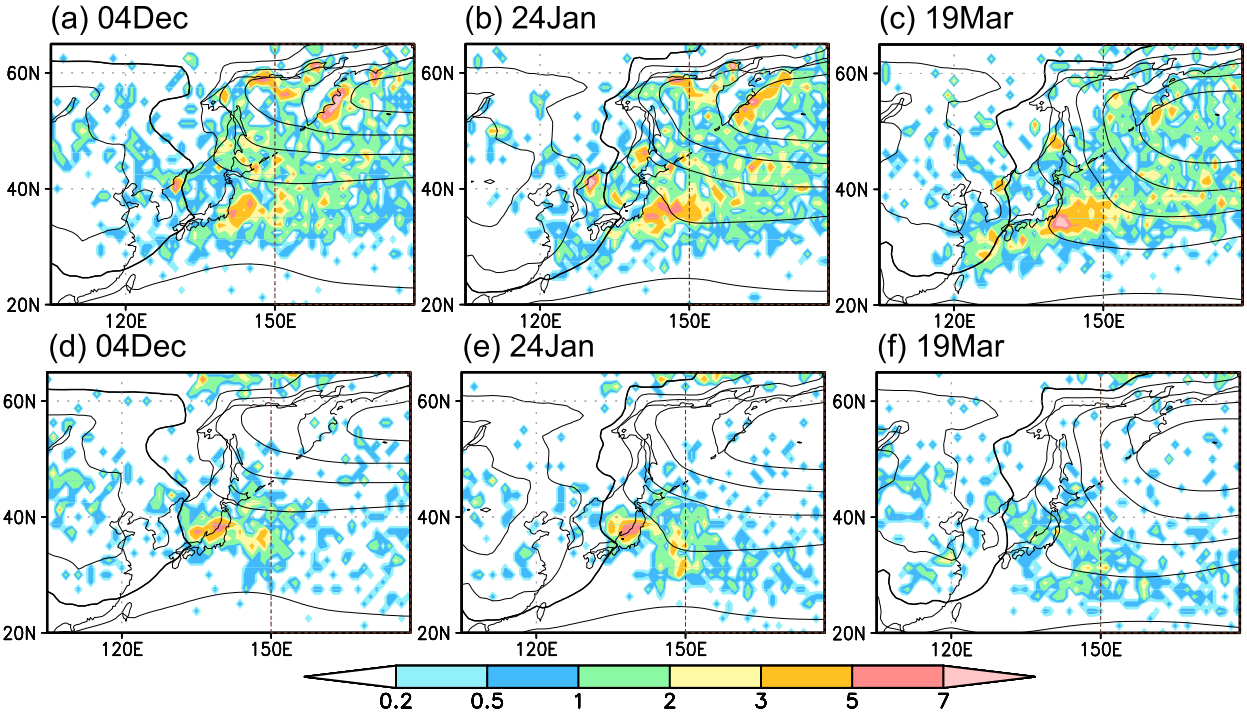

FIG. 4. (a)–(c) Climatological-mean density (×0.01%) of the genesis of surface cyclones that pass through the domain of 20°–65°N, 150°E–150°W, over the central NP for the calendar days as indicated. Black contours denote climatological-mean SLP (every 4 hPa). (d)–(f) As in (a)–(c), respectively, but for the genesis of identified anticyclones.

from the ECS is also more frequent in spring. These cyclone paths seem to correspond to the two branches of the upper-level disturbances pointed out by Chang (2005), and they are also consistent with Schemm et al. (2021). Another noticeable aspect is that the number of cyclones propagating from northern China (especially west of 120°E) decreases in midwinter (Fig. 3b). This is suggestive of reduced cyclone activity along ~50°N over East Asia, and consistent with the prominent midwinter reduction in the number of upper-level cyclonic disturbances over the NP originated over land as pointed out by Penny et al. (2010). They may be compared with upper-level cyclonic disturbances originating over the NP, whose number exhibits no prominent MWM and peaks in spring (Penny et al. 2010).

The NP anticyclones are likely to propagate from the Japan Sea in early winter and spring (Figs. 3d,f). This typical pathway is consistent with the climatologies for SON, DJF, and MAM obtained by Pepler et al. (2019). The propagation is greatly suppressed in midwinter (Fig. 3e), suggestive of an important contribution of anticyclones traveling from the Japan Sea for the NP anticyclone density. The high density around the Yellow Sea may be due to rather slow movement of anticyclones (not shown) after separated from the Siberian high, as hinted by climatological-mean SLP contours (Fig. 3f).

To further investigate the origin of the NP cyclones and anticyclones, the frequency of their geneses is shown in Fig. 4. Cyclogenesis occurs most frequently over the KE and around the Kamchatka Peninsula. The latter signifies cyclones generated locally around the peninsula, and their number decreases in spring, when cyclogenesis over the ECS becomes more frequent (Fig. 4c). These results are consistent with Schemm et al. (2021), and the frequent midwinter cyclogenesis over the KE is in agreement with Masunaga et al. (2020). In contrast, genesis of anticyclones is most likely around Japan. In early winter and midwinter, the genesis is most frequent over the central Japan Sea (Figs. 4d,e). In spring (Fig. 4f), genesis around Japan becomes less frequent, implying that the high anticyclone density over the Japan Sea in Fig. 3f is due to genesis around the northwestern Japan Sea or farther upstream over China (west of 120°E).

The results obtained thus far suggest that anticyclones around the Japan Sea can be important for the seasonality of anticyclone density over the NP. To assess the influence on the NP storm-track activity from upstream, the densities of cyclones and anticyclones shown in Fig. 2 for the NP are decomposed into those due to such cyclones and anticyclones that have passed through the domain (35°–42°N, 130°–140°E) over the Japan Sea (JPS) and the residuals (Fig. 5). As evident in Fig. 5b, the dual peaks of the NP anticyclone density in autumn and spring as well as its distinct MWM are explained exclusively by anticyclones coming from upstream. This can be confirmed also by the nearly constant density of the residual anticyclones throughout the cold season (Fig. 5d). In autumn, anticyclones generated over the JPS are more important than in spring, which is consistent with Fig. 4d. In spring, anticyclones passing through the JPS are more likely to reach the North Pacific (Fig. 4f).

By contrast, cyclones coming from the JPS domain exert only modest influence on the seasonality in the NP cyclone

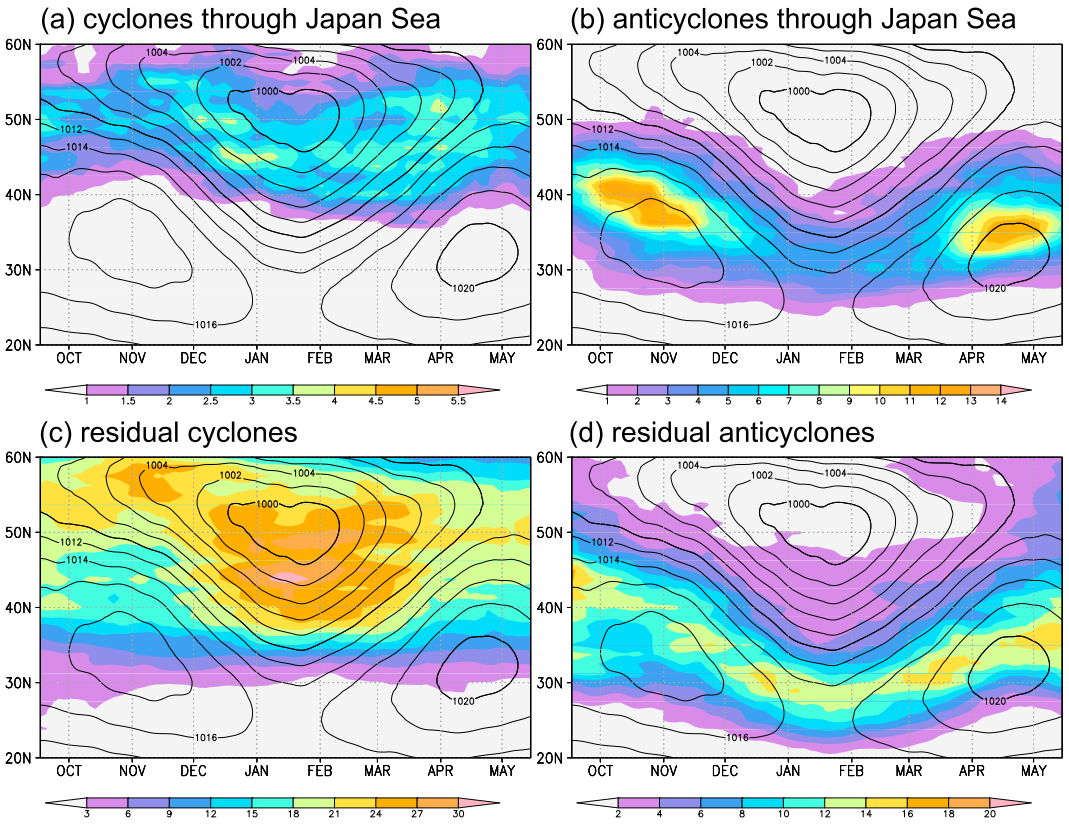

FIG. 5. (a),(b) As in Figs. 2a and 2b, respectively, but for identified cyclones and anticyclones that pass through the domain of 35°–42°N, 130°–140°E over the Japan Sea (JPS) during their lifetimes. (c),(d) As in (a) and (b), respectively, but for cyclones and anticyclones that *do not* pass through the JPS domain during their lifetimes.

density in Fig. 2a if compared to the residual (Figs. 5a,c). Although migratory cyclones are more numerous from early to midwinter along ~41°N over the JPS domain (not shown), a substantial fraction of those cyclones must be meso-α-scale cyclones that develop within monsoonal cold airflows associated with upper-level cold cyclonic vortices, which are most frequent in January (Yanase et al. 2016; Watanabe et al. 2018).

Activity of synoptic-scale disturbances is strongly influenced by upper-tropospheric eddies (Takayabu 1991). To examine the seasonality of upper-level eddy activity, frequencies of cyclonic and anticyclonic vortices are evaluated with a method based on local curvature introduced by ONK21 (see section 2 in supplementary material for more details). The curvature thresholds are set to be $\pm 4 \times 10^{-7}$ m^{-1} for cyclonic and anticyclonic vortices, respectively, which correspond to circulation with radius less than 2500 km. Note that this method is unlikely to be influenced strongly by the actual size of an individual migratory trough or ridge, because their radii must be smaller than 2500 km. Nevertheless, the result is qualitatively similar when centers of vortices (equivalently, local extrema of curvature) are tracked in an analogous manner to the surface tracking algorithm (see supplementary Fig. S3). The result is also qualitatively similar with a threshold radius of 1000 km.

Both in the western NP (Fig. 6a) and JPS (Fig. 6c) sectors, cyclonic vortices are less frequent around the axis of the upper-tropospheric westerly jet stream and its southern flank than to the north, in good agreement with ONK21. The probability of upper-level cyclonic vortices peaks in midwinter at ~45°N and to the north, where the surface cyclone density also maximizes over the central NP (Fig. 2a). This is also consistent with Watanabe et al. (2018), who showed that a surface meso-α-scale cyclone in midwinter over the Japan Sea tends to be accompanied by an intense free-tropospheric pressure trough. In comparison, upper-level anticyclonic vortices tend to be less frequent in the extratropical western NP (Figs. 6b,d), except along the southern flank of the jet stream in autumn and spring. The MWM of frequency of anticyclonic vortices is evident over both the NP and JPS sectors, which is consistent with the suppressed activity of surface anticyclones.

The result showing the midwinter maximum (minimum) of the frequency of upper-tropospheric cyclonic (anticyclonic) vortices over the JPS sector may apparently be inconsistent with Penny et al. (2010), who showed that the "seeding effect" on the NP storm track from the upstream is less effective in midwinter than in the shoulder seasons, based on a tracking of negative anomalies of high-pass-filtered 300-hPa height. The apparent discrepancy between the results in this study and theirs may be due to the difference in the scopes and ways of identifying upper-level disturbances. Specifically, Penny et al. (2010) attempted to relate 300-hPa height anomalies to the variance of

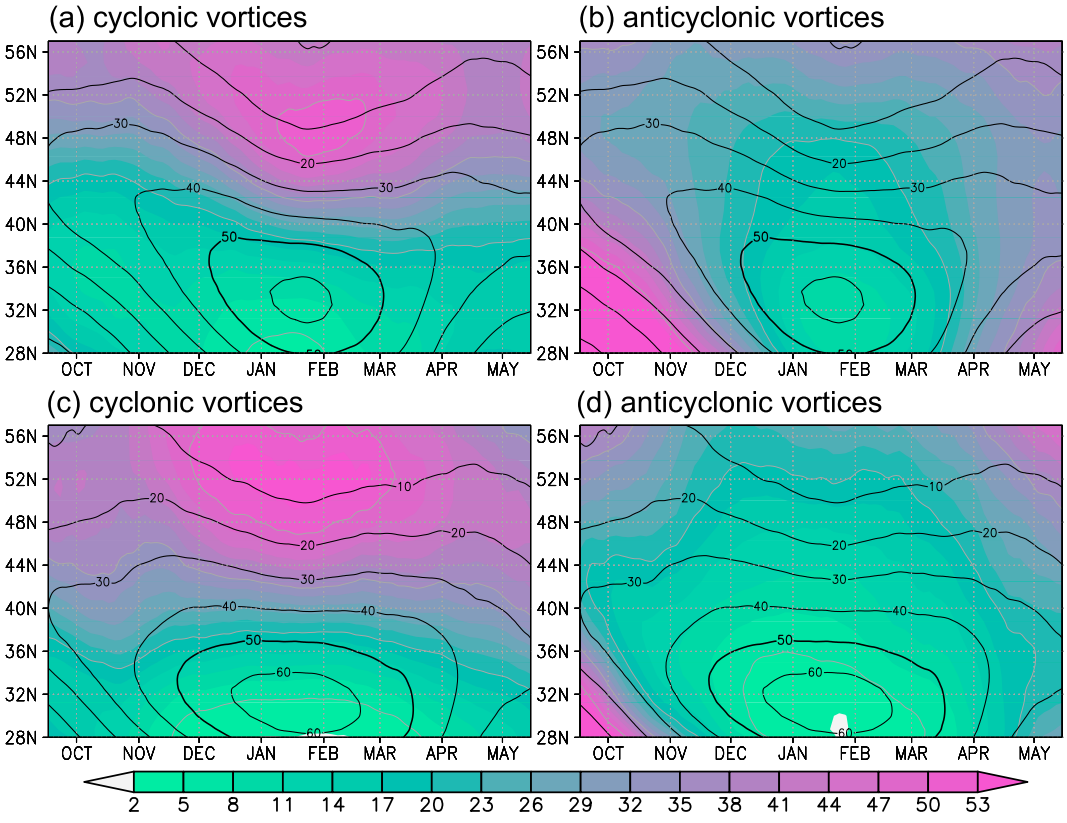

FIG. 6. Latitude–season sections of climatological-mean probability (colors; %) of domains of (a) cyclonic and (b) anticyclonic vortices at 300-hPa based on curvature. Grid points where instantaneous curvature radius is smaller than 2500 km are counted as domains of cyclonic or anticyclonic vortices depending on their sign. Contours indicate climatological-mean U_{300} (every 10 m s^{-1}). All the quantities plotted are averaged zonally between 150°E and 180° over the western North Pacific. (c),(d) As in (a) and (b), respectively, but for probability averaged between 130° and 140°E.

high-pass-filtered geopotential height. In this study, by contrast, local curvature is calculated from unfiltered horizontal winds to be consistent with the tracking of surface cyclones and anticyclones based on the unfiltered SLP fields. We consider that they are systems having their own structures in the total (unfiltered) field, which interact with and include the influence from low-frequency variabilities and climatological background states. Besides, our 300-hPa curvature tracking applied to a sector west of 130°E indicates that the frequency of cyclonic vortices does not maximize in midwinter, but rather is slightly reduced between the peaks in the shoulder seasons north of ~40°N (not shown), which is compatible with the seasonality downwind of the Tibetan Plateau by Penny et al. (2010). These results suggest that the "seeding effect" from upstream is effective in the seasonality not of surface migratory cyclones but of anticyclones over the JPS domain, leading to the midwinter minimum of anticyclone density over the NP (Fig. 2).

Section summary

The following are the two most important outcomes from section 3.

- Over the NP, the anticyclone density minimizes in midwinter, while the cyclone density maximizes in midwinter.
- The midwinter reduction in anticyclones over the NP is explained exclusively by those coming from the Japan Sea.

4. Composite analysis for anticyclones over the Japan Sea

In section 3, we have demonstrated that anticyclones from the JPS domain are of critical importance for the seasonality of anticyclone density over the NP. To elucidate the structure and associated environment for those anticyclones, Figs. 7a–c show a composited three-dimensional structure of those anticyclones moving over the JPS domain for the three calendar days after shifting their surface centers horizontally in such a manner that they are all located at the origin of the coordinates. The composited SLP fields (Figs. 7a–c) suggest features of a synoptic-scale anticyclone separated from the climatological-mean Siberian high. The typical vertical structure of the composited anticyclonic anomalies over the JPS region is shown in Figs. 7d–f, as latitudinal averages of high-pass-filtered geopotential height and temperature from 10° south to 10° north of the composited centers. Those figures highlight westward-tilting height anomalies with altitude, indicating their baroclinic structure. The midwinter JPS surface

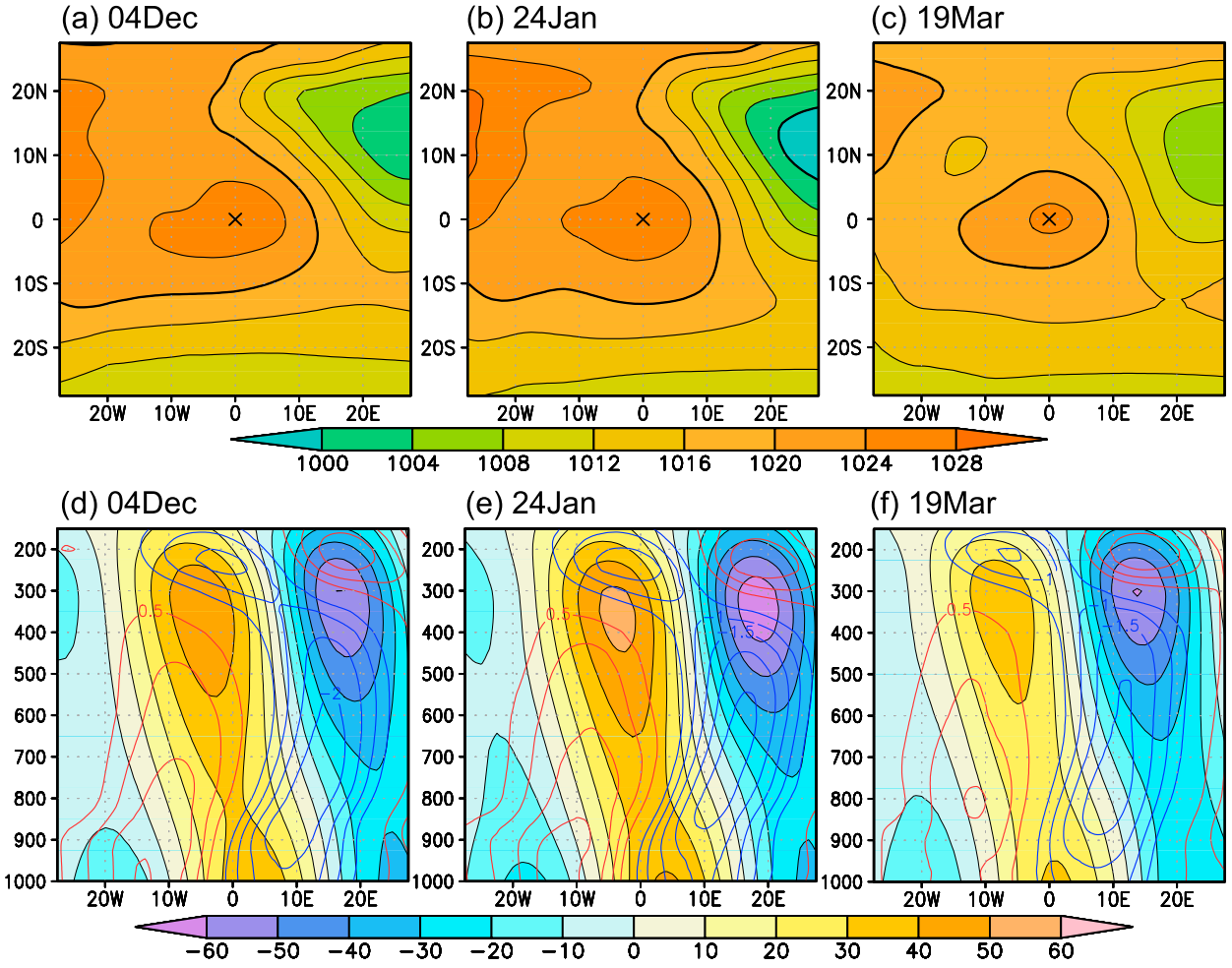

FIG. 7. (a)–(c) Composited fields of unfiltered SLP (hPa) based on the surface anticyclone centers identified over the Japan Sea domain (35°–42°N, 130°–140°E) for the calendar days as indicated. Before the compositing, all selected SLP fields have been shifted horizontally in such a manner that the surface anticyclone centers are collocated at a grid point as indicated in each of the panels and marked with a black cross. Labels on the abscissa and ordinate denote longitude and latitude (°), respectively, relative to the center. (d)–(f) Zonal sections of the composited high-pass-filtered anomalies in geopotential height (colors; m) and temperature (colored contours; K) for the surface anticyclones for the indicated calendar days. In each panel, variables are averaged over a 20° latitudinal band centered at the latitude of an identified surface anticyclone center.

anticyclones tend to be accompanied by stronger upper-tropospheric height anomalies (Fig. 7e) than their counterpart in the shoulder seasons (Figs. 7d,f), which is not the case for surface cyclones over the JPS (not shown).

A question arising here is what kind of background field is favorable for a surface anticyclone to exist over the JPS. In computing a composited SLP field at time steps when a surface anticyclone is located over the midwinter JPS, we noticed that SLP over the Asian continent tends to be lower than the climatology (not shown), indicative of the weakened Siberian high. To investigate an anomalous background state for a JPS anticyclone, we composite low-pass-filtered anomaly fields of a given variable X defined as $[X]_L \equiv [X] - [X'] - X_C$, where $[X]$ denotes a composited field, a prime a high-pass-filtered field, and the subscript C the climatological mean. Note that this decomposition assumes that a low-frequency anomaly can be separated from a synoptic-scale disturbance. Figure 8 shows $[Z_{300}]_L$ and $[T_{850}]_L$ when an anticyclone exists over the JPS domain. In midwinter (Fig. 8b), an anticyclonic $[Z_{300}]_L$ anomaly spreading over midlatitude East Asia is indicative of the weakened climatological-mean East Asian trough. The corresponding warm anomaly over East Asia indicates that the East Asian cold monsoonal airflow is weaker associated with a surface JPS anticyclone (Fig. 8e). Furthermore, those low-frequency anomalies are strongest in midwinter (Fig. 8). These results indicate that the marked weakening of the climatological-mean upper-level East Asian trough and monsoonal cold surge is needed in midwinter for a surface anticyclone to be cut off from the Siberian high into the JPS domain. This seasonality implies that migratory anticyclones over the JPS domain are less likely in midwinter under seasonally enhanced monsoonal cold surge.

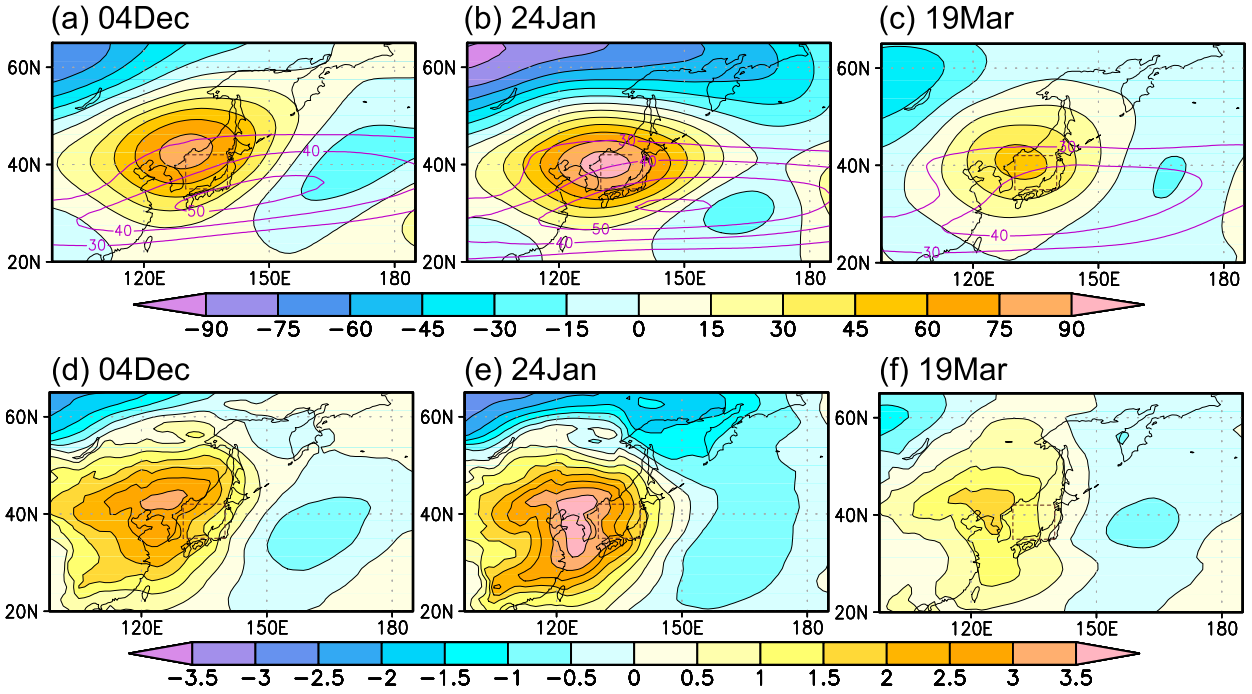

FIG. 8. (a)–(c) Composite maps of low-frequency anomalies of 300-hPa geopotential height (colors; m) at time steps when one or more anticyclonic centers are located over the Japan Sea domain (35°–42°N, 130°–140°E; indicated with dashed rectangles) for the calendar days as indicated. Purple contours indicate composited low-frequency component of U_{300} (m s^{-1}). (d)–(f) As in (a)–(c), respectively, but for low-frequency anomalies of temperature at 850 hPa (K).

To investigate upstream influence on the low-frequency height anomaly over midlatitude East Asia, a wave-activity flux defined by Takaya and Nakamura (2001) is utilized. The low-frequency anticyclonic anomaly in the upper troposphere is influenced by wave-activity injection from the upstream (Figs. 9a–c). Wave-activity flux extends over Siberia through a cyclonic anomaly at ~100°E especially in midwinter. These cyclonic and anticyclonic anomalies are quasi stationary and roughly along the polar-front jet, as seen in lag-composite maps by three days, especially in early to midwinter (Figs. 9d–f). The wave train resembles the Eurasian teleconnection (EU) pattern (Wallace and Gutzler 1981), which is one of the dominant teleconnection patterns in the wintertime Northern Hemisphere. Actually, the wave train shown in Fig. 9e resembles the composite map at lag −3 days based on the EU pattern index (Wang and Zhang 2015). The wave train also resembles the Scandinavian pattern in January (Bueh and Nakamura 2007). In addition, a similar wave train but with the reversed polarity is observed in blocking events around 57°N, 80°E in association with the intensified surface Siberian high (Takaya and Nakamura 2005), suggesting the potential influence by the upstream wave train from the Euro-Atlantic sector on low-frequency variability in the Siberian high and East Asian winter monsoon.

To investigate the vertical structure of the low-frequency anomalies associated with JPS surface anticyclones, meridional sections are constructed by taking a zonal average between 130° and 140°E. As evident in Figs. 10a–c, the low-frequency anomalies are characterized by dipolar anomalies in upper-level zonal winds. The westerlies are anomalously weakened around the jet core and enhanced to its north, representing a poleward widening of the jet. These low-frequency wind anomalies associated with the JPS surface anticyclones are strongest in midwinter (Fig. 10b), rendering the jet structure in midwinter similar to that often observed in the shoulder seasons (Figs. 10a,c). Consistently, the dipolar upper-level wind anomalies accompany a warm anomaly over the JPS throughout the depth of the troposphere, capped by a cool anomaly at the tropopause level (Figs. 10d–f). Again, these thermal anomalies are maximized in midwinter. Associated with these anomalies, static stability is lowered by ~20% and thus the Rossby depth ($\equiv fL/N$, with horizontal scale L and the Brunt–Väisälä frequency N) increases, especially in the midtroposphere.[3] Due to the combined effects of the

[3] One may consider that L can be scaled with the Rossby depth. To test this, the penetration depth of baroclinic instability $h = (f^2/N^2)[(\partial\overline{u}/\partial z)/(\partial\overline{q}/\partial y)]$ defined by Held (1978) is also estimated. It may be expressed as $h = H/\{1 + (N^2H/f^2)[\beta/(\partial\overline{u}/\partial z)]\}$ for the Charney mode, where H denotes the scale height. With the seasonal displacement of the jet axis, midtropospheric $\partial\overline{u}/\partial z$ is maximized in midwinter to the south of ~40°N but reduced to the north relative to the shoulder seasons, resulting in only weak differences in h around the low-frequency temperature anomaly over the JPS domain (not shown). It is therefore suggested that the consideration of the scaling of L with the Rossby depth is unlikely to alter the argument substantially.

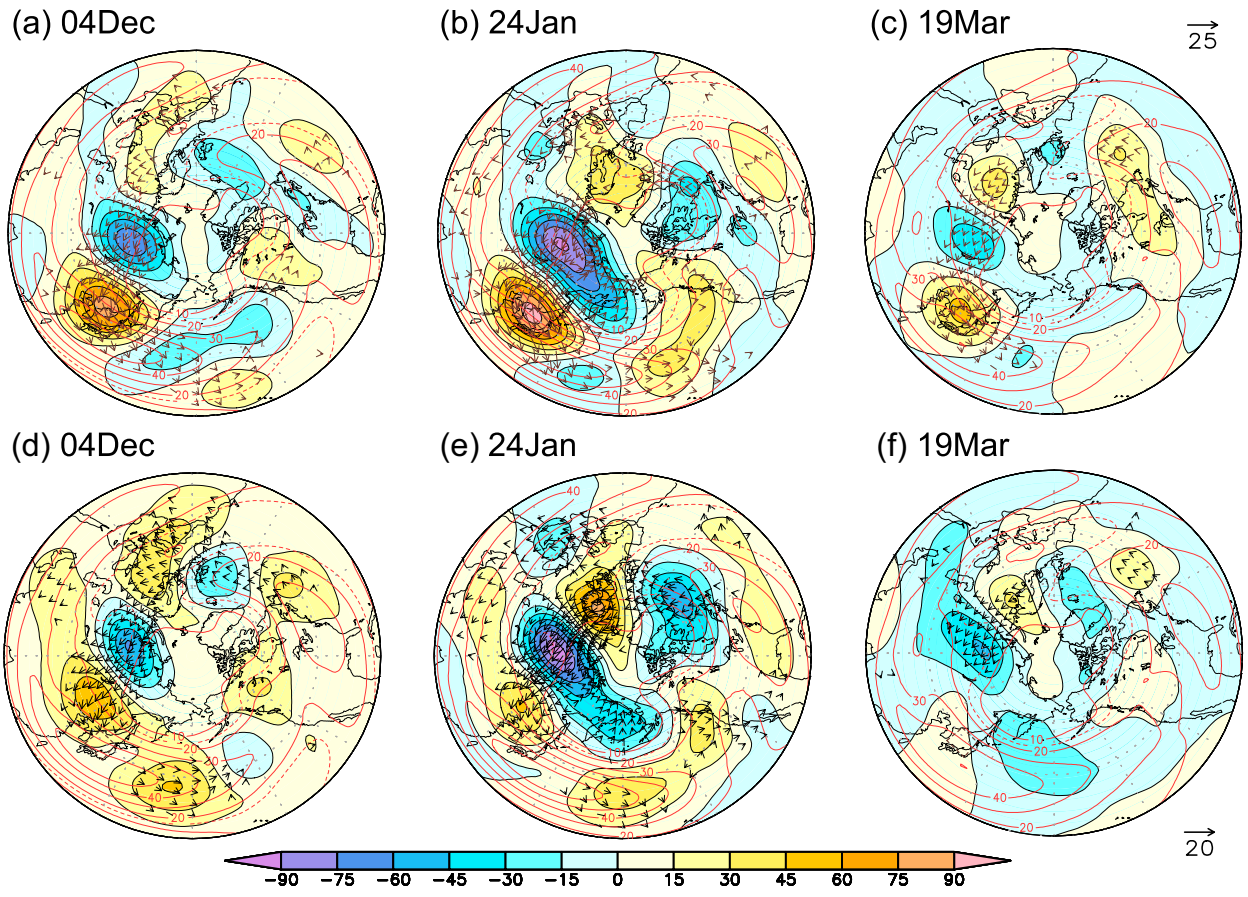

FIG. 9. (a)–(c) Composite map of low-frequency anomalies of 300-hPa geopotential height (colors; m) at time steps when one or more anticyclonic centers are located over the Japan Sea domain (indicated with dashed rectangles) for the calendar days as indicated. Red contours signify the climatological-mean westerly wind speed (m s^{-1}). Vectors indicate a Rossby wave-activity flux (m^2 s^{-2}) at 300 hPa defined by Takaya and Nakamura (2001). (d)–(f) As in (a)–(c), respectively, but for time steps leading those in (a)–(c) by 3 days.

midwinter anomalies on the lower static stability and weaker jet intensity, trapping effect of upper-level eddies into the jet core in midwinter tends to be weakened and thus upper-tropospheric eddies tend to be linked more strongly with the lower-tropospheric anomalies for their baroclinic development (Nakamura and Sampe 2002).

As the midwinter climatology (Fig. 11b), vertical gradient of potential temperature, corresponding to static stability, is pronounced at the tropopause level to the north of the jet core, while it is relatively low in the free troposphere over the JPS sector and much lower near the surface. Compared with the midwinter situation, static stability tends to be slightly lower in the mid- and upper troposphere in the shoulder seasons (Figs. 11a,c), suggesting the climatologically greater Rossby depth. The midwinter maximum of midtropospheric static stability, which seems consistent with the result obtained by Frierson and Davis (2011) from a zonal-mean perspective, probably reflects seasonally enhanced cold surge from the stronger Siberian high (Zhang et al. 1997). The reduced Rossby depth acts to retard the vertical connection of upper-tropospheric eddies with lower-tropospheric eddies, which can contribute to less frequent surface anticyclones over JPS together with fewer upper-tropospheric anticyclonic vortices. The discussion is consistent with the tendency for upper-tropospheric eddies to be trapped in the jet core and thus less connected with the surface baroclinic zone anchored by the midlatitude oceanic frontal zone, as argued by Nakamura and Sampe (2002). In addition, excessively strong vertical shear of the westerlies in midwinter (viz., small Richardson number) may render the vertical scale of eddies smaller than the corresponding Rossby depth, as a characteristic of nongeostrophic baroclinic instability as indicated by Nakamura (1988). The retarded vertical linkage of upper-tropospheric vortices with surface anticyclones can be seen in the fractional amplitude of the composited lower-tropospheric $[Z]'$ relative to the upper-tropospheric eddies (Figs. 11d–f). In midwinter, the relative amplitude of low-level anticyclonic eddies is indeed smaller than in the shoulder seasons, which is consistent with Nakamura and Sampe (2002). The vertical connection becomes more prominent in spring (Fig. 11f), but the difference between early and midwinter is much less distinct, as also noticeable in Figs. 8–10 and 11a–c. This may apparently be inconsistent with the frequent anticyclogenesis over the early winter JPS (Fig. 4d). This seasonality may be

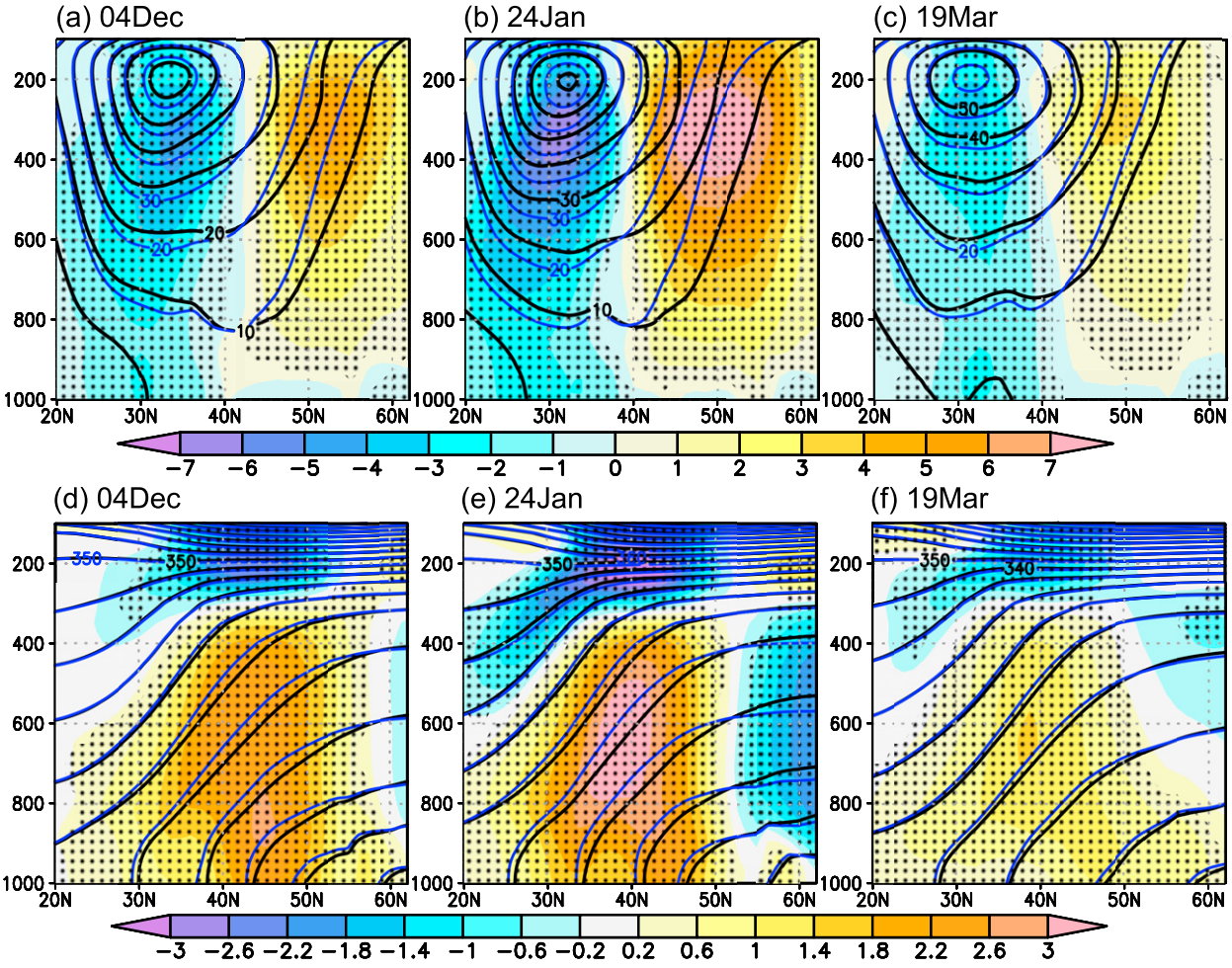

FIG. 10. (a)–(c) Meridional sections of composited low-frequency anomalies of westerly wind speed (colors; m s^{-1}) at time steps when one or more anticyclonic centers are located over the Japan Sea domain for the calendar days as indicated. Black and blue contours indicate composited low-frequency component and climatological mean of westerly wind speed, respectively (every 10 m s^{-1}). All the quantities plotted have been averaged between 130° and 140°E. Stippling indicates statistically significant difference at the 95% confidence level based on a random subsampling of time steps by 5000 times, the number of which is the same as that of anticyclones used for respective composites (viz., 176, 114, and 226), within the entire time steps used for 31-day running-mean climatologies around the respective calendar days of individual years (i.e., 31 × 4 × 59). (d)–(f) As in (a)–(c), respectively, but for low-frequency anomalies of potential temperature (colors; K). Black and blue contours indicate composited low-frequency component and climatological-mean potential temperature, respectively (every 10 K).

attributable to stronger lower-tropospheric meridional temperature gradient over the JPS in autumn than in spring, which corresponds to the stronger meridional SST gradient over the JPS in autumn (not shown).

One may wonder whether the above argument can also apply to the midwinter reduction in the JPS cyclones or not. Midwinter weakening of the vertical linkage is indeed also found in the corresponding composites for cyclonic vortices in the JPS domain (not shown). Nevertheless, the frequency of the JPS cyclones does not exhibit a clear MWM between the peaks in early winter and spring. The relatively frequent cyclogenesis over the midwinter JPS may be attributable to meso-α-scale cyclones, whose formation is related more to diabatic processes over relatively warm SST under cold free-tropospheric anomalies (Yanase et al. 2016). This is consistent with the much weaker low-frequency anomalies associated with the JPS cyclones than anticyclones (supplementary Figs. S4 and S5).

Section summary

The following are the three most important outcomes from section 4.

- Surface anticyclones over the Japan Sea tend to accompany low-frequency low-level warm anomalies and upper-level anticyclonic anomalies, which correspond to the weakening of the monsoonal airflow and act to enhance the vertical coupling of migratory eddies.
- The climatologically strong retardation of the vertical coupling in midwinter requires markedly strong low-frequency

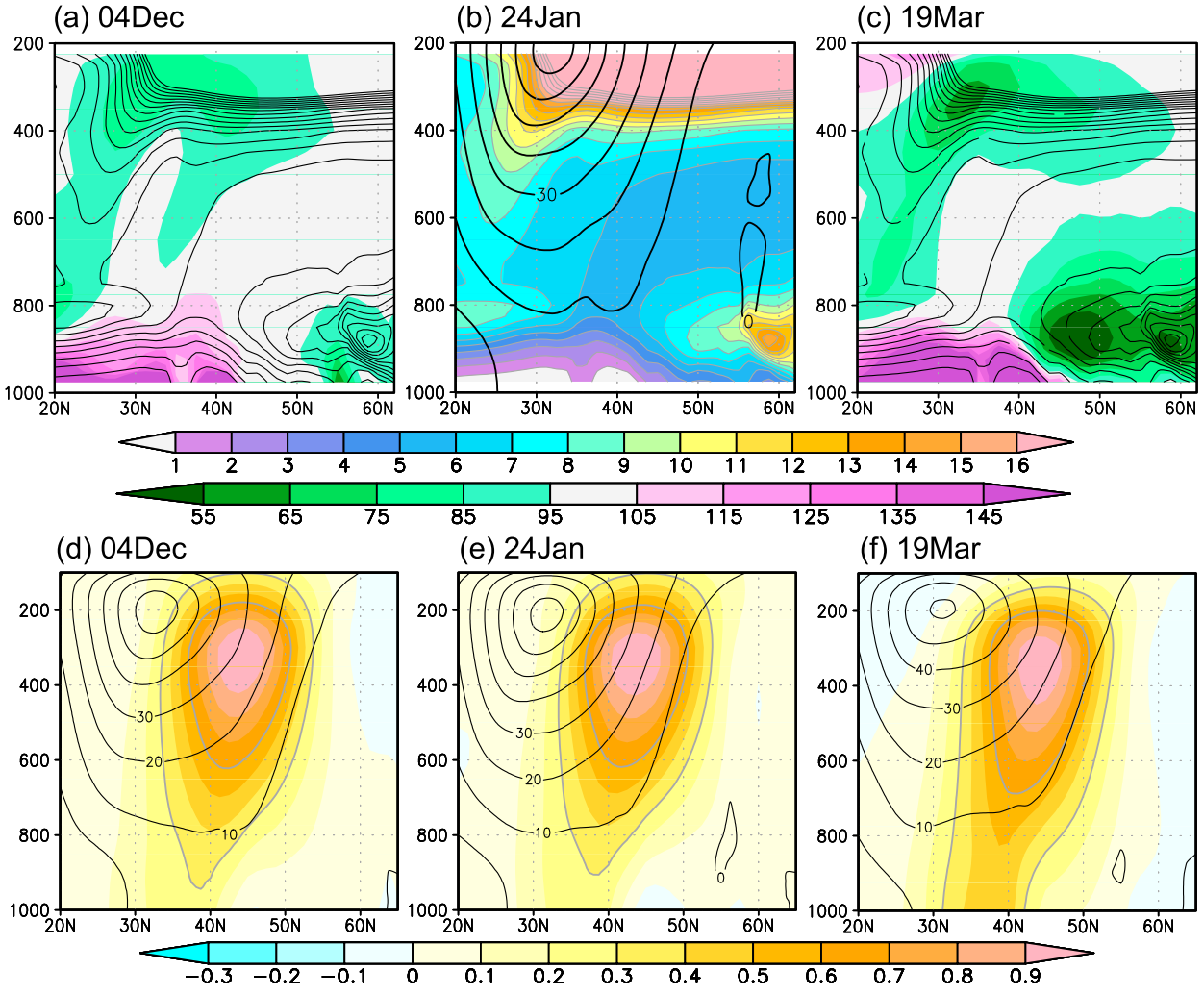

FIG. 11. (a) Ratio of climatological-mean vertical gradient of potential temperature for 4 Dec to that for 24 Jan (colors; %). Black contours are identical to gray contours in (b). (b) Meridional sections of the climatological-mean vertical gradient of potential temperature [colors; K (100 hPa)$^{-1}$] and westerly wind speed (black contours; every 10 m s^{-1}) for 24 Jan. (c) As in (a), but for the climatological mean for 19 Mar. All the quantities plotted have been averaged between 130° and 140°E. (d)–(f) Meridional sections of the ratio of composited high-pass-filtered anomalies of geopotential height to the maximum value between the 500- and 100-hPa levels (colors) at time steps when one or more anticyclonic centers are located over the Japan Sea domain for the calendar days as indicated. The ratios of 0.3 and 0.6 are highlighted by gray contours. Black contours indicate climatological-mean westerly wind speed (every 10 m s^{-1}). All the quantities plotted have been averaged between 125° and 135°E.

anomalies for migratory surface anticyclones to exist over the Japan Sea, leading to the midwinter reduction in their frequency.

- The upper-level low-frequency anticyclonic anomaly is related to an EU-pattern-like wave train over Eurasia.

5. Long-term modulations of the MWM

In this section, we briefly describe long-term modulations of densities of cyclone and anticyclone centers and associated background states. Following Nakamura et al. (2002), we divide the entire analysis period into the earlier (1958/59–1985/86) and later (1986/87–2016/17) periods. The earlier (later) period is characterized by a stronger (weaker) suppression of the midwinter NP storm-track activity (Nakamura et al. 2002). Note that results for the long-term modulations of frequency of surface cyclones/anticyclones are qualitatively the same when the latter period is extended to 2020/21. Note also that similar results can be obtained with JRA-55C (Kobayashi et al. 2014), in which only conventional observations are assimilated.

The two periods are marked basically by the midwinter maximum in cyclone density and the MWM in anticyclonic density over the western NP (Fig. 12) as seen for the entire period, suggestive of the robustness of the characteristics. Comparison between the two periods reveals, however, that the seasonality of cyclone and anticyclone densities shows

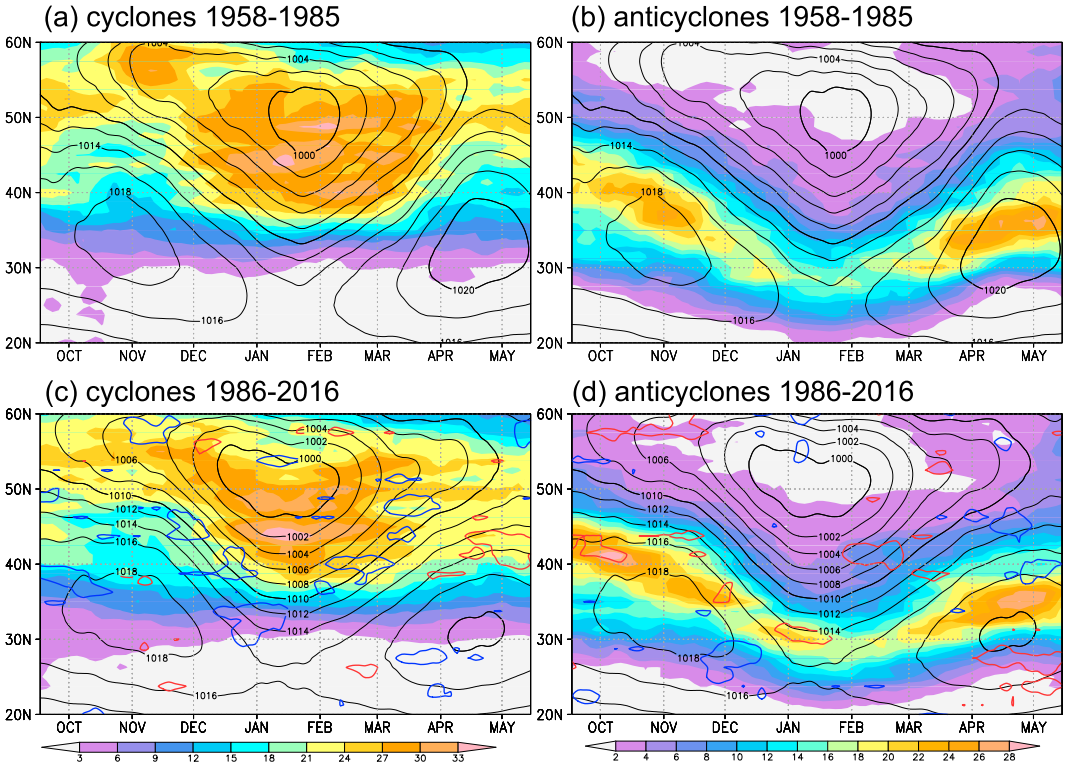

FIG. 12. As in Fig. 2, but for probability in (a),(b) the earlier period (1958/59–1985/86) and (c),(d) the later period (1986/87–2016/17). Red and blue contours in (c) and (d) denote statistically significant increase and decrease, respectively, from the former period at the 90% confidence level by Student's *t* test.

long-term modulations. In the earlier period (Fig. 12a), southward expansion of the region of high cyclonic density persists longer than in the later period (Fig. 12c). In addition, in the earlier period (Fig. 12b), the MWM of anticyclonic density is more distinct, and the axis of its maximum density migrates farther equatorward when compared to the later period (Fig. 12d). It may be related to the enhanced equatorward expansion of the AL as well as the southward-shifted and weakened subtropical high pressure belt in midwinter in the earlier period (black contours in Fig. 12). This is consistent with the interdecadal modulations of the East Asian winter monsoon shown by previous studies (Nakamura et al. 2002; Wang et al. 2009).

The interpretation presented in the preceding section can also apply to the long-term modulations of anticyclonic density. Figures 13a and 13d show the density of surface anticyclones over the NP that have passed through the JPS domain as in section 4. Evidently, the contribution of anticyclones coming from the JPS domain to the MWM of the NP anticyclone density is more distinct during the earlier period. Though less significant, residual anticyclones increased in the later period, which also contributed to the weakening of the MWM in the total density over the NP (Figs. 13b,e). In contrast, the seasonal evolution of the density of residual cyclones over the NP is similar to that of the total density (Figs. 12 and 13), with a significant reduction into the later period. This result suggests that cyclones passing through the JPS domain may not be quite relevant to shaping the midwinter maximum of the NP cyclone density.

In the later period, the wintertime NP upper-tropospheric westerly jet has widened poleward compared to the earlier period over the East Asian sector (Figs. 14a–c), which is consistent with previous studies (e.g., Archer and Caldeira 2008). Though not statistically significant, the widening in the mid- and upper troposphere is most prominent in midwinter, while lower-tropospheric westerly intensification to the north of ~40°N is comparable between midwinter and early spring. Compared to the shoulder seasons, the corresponding long-term modulations of potential temperature are marked in midwinter with more rapid warming to the north (south) in the lower (upper) troposphere and the tropopause-level cooling especially to the north of 50°N (Figs. 14d–f). The warming in the lower- to midtroposphere is statistically significant, especially in midwinter. It acts to attenuate the midtropospheric stratification below the westerly jet axis and over the JPS domain, leading to an increase in Rossby depth. In other words, the retardation of the vertical connection of upper-tropospheric eddies with near-surface disturbances in midwinter has been somewhat relaxed in the later period, which is consistent with the suggestion by Nakamura and Sampe (2002).

6. Summary and discussion

In this study we have investigated the detailed seasonal evolution of frequency of migratory surface anticyclone centers over the NP, in comparison with its cyclonic counterpart,

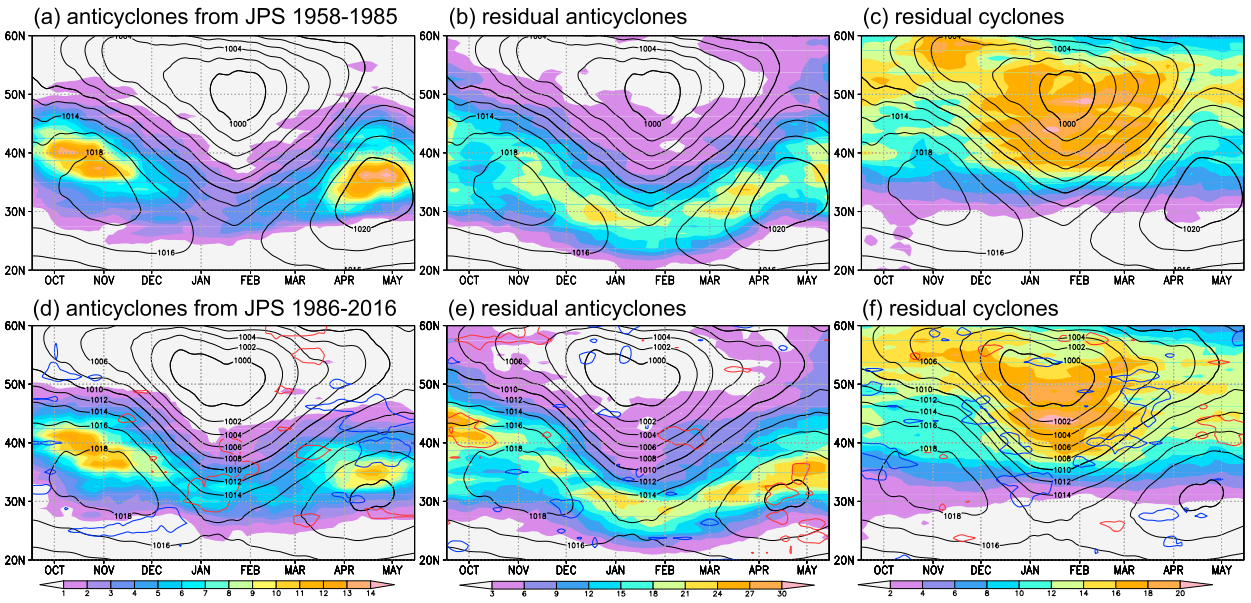

FIG. 13. (a)–(c) As in Figs. 5b, 5d, and 5c, respectively, but for probability in the earlier period (1958/59–1985/86). (d)–(f) As in (a)–(c), respectively, but for probability in the later period (1986/87–2016/17). Red and blue contours in (d)–(f) denote statistically significant increase and decrease, respectively, from the former period at the 90% confidence level by the Student's *t* test.

based on the feature tracking algorithm described in section 2. We have revealed that the seasonality of those surface anticyclones is distinctively different from that of surface cyclones. Additionally, we have also revealed that the seasonality of the surface anticyclone density around the NP storm track is substantially under the upstream influence, especially from the JPS domain located at the storm-track entrance.

In the shoulder seasons, density of migratory surface anticyclones is found relatively high over the JPS domain under the frequent passage of upper-tropospheric anticyclonic vortices and relatively low midtropospheric static stability. Some of those anticyclones propagate into the NP storm-track region to form the two distinct peaks in the seasonal density of migratory anticyclones. In midwinter, by contrast, density of surface anticyclones over JPS is lower under the less frequent passage of upper-tropospheric anticyclonic vortices and higher midtropospheric static stability in association with the monsoonal cold-air outbreaks and the excessively strong westerly jet stream. In this circumstance, the vertical coupling between upper- and lower-tropospheric eddies tends to be retarded (Nakamura and Sampe 2002), leading to the distinct density minimum of migratory anticyclones over the NP. This is apparently inconsistent with baroclinic instability theory, in that activity of migratory eddies and their vertical coupling minimize when the vertical shear of westerly wind speed maximizes.

Our composite analysis for migratory anticyclones over the JPS domain indicates that they tend to be accompanied by persistent weakening of the climatological East Asian trough associated with upper-level planetary waves and associated lower-tropospheric warming. The weakening of the East Asian winter monsoon tends to be preceded by Rossby wave propagation from upstream. Midwinter anticyclones moving over the JPS domain are likely to be accompanied by stronger, more distinct low-frequency anomalies than in the shoulder seasons. This suggests that a more prominent, unusual weakening of the winter monsoon is needed for a migratory anticyclone over the JPS domain to form under the unfavorable climatological-mean condition, which is consistent with the climatologically fewer migratory anticyclones over the midwinter NP.

In sharp contrast to the seasonality of anticyclone density, density of migratory cyclones over the NP is maximized in midwinter, which is compatible with the baroclinic instability theory. It may be explained largely by local cyclogenesis around the Kamchatka Peninsula, Kuroshio Extension, and cyclones propagating from the East China Sea, rather than that over the JPS domain (Fig. 5c). Consistently, upper-tropospheric cyclonic vortices aloft tend to be observed more frequently in midwinter.

Additionally, we have confirmed that the above discussion can be overall applied to interdecadal modulations of the MWM of the NP storm-track activity. In the more recent period after the mid-1980s, the MWM became less distinct both in the NP storm-track activity and NP anticyclone density, the latter of which may be related to the more frequent surface anticyclones over the JPS domain under the lowered midtropospheric static stability. During this period, the midwinter density of NP migratory cyclones became lower. Though still obvious, its midwinter maximum becomes slightly less distinct.

The fact that anticyclones are less frequent over the midwinter NP in contrast to the midwinter maximum of cyclone density suggests that anticyclones are likely the key to the understanding of the MWM of the NP storm-track activity, as

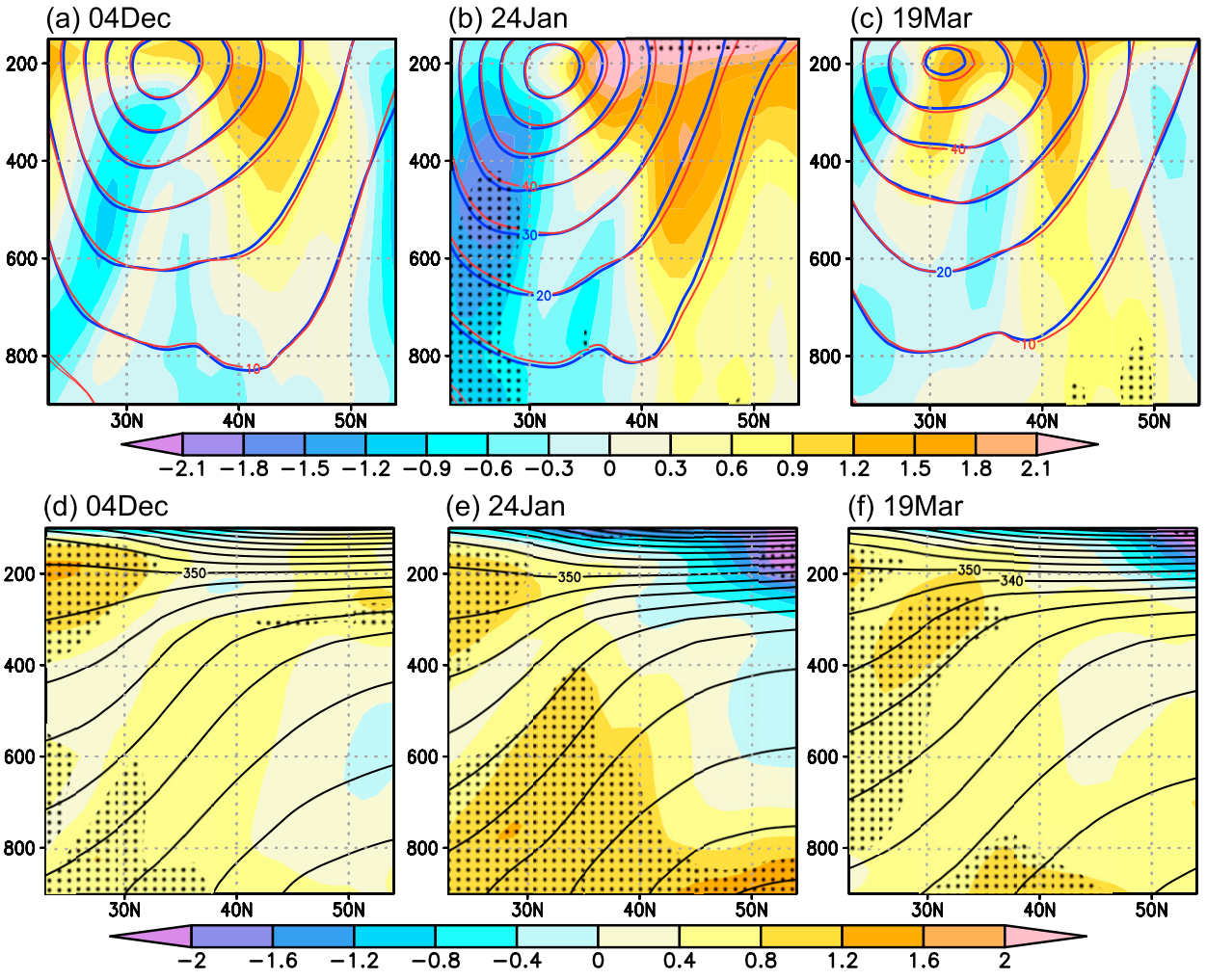

FIG. 14. (a)–(c) Differences in climatological-mean westerly wind speed (colors; m s^{-1}) averaged for 130°–140°E between the earlier (1958–85) and later (1986–2016) periods. Blue and red contours denote climatological-mean westerly wind speed (m s^{-1}) in the earlier and later periods, respectively. Stippling indicates statistically significant differences at the 90% confidence level by the Student's t test. (d)–(f) As in (a)–(c), but for the corresponding difference in climatological-mean potential temperature (colors; K). Black contours denote climatological-mean potential temperature (K) in the later period.

measured by Eulerian eddy statistics (Nakamura 1992). Indeed, our preliminary results show that the anticyclonic contribution plays a pivotal role in setting the MWM of Eulerian eddy statistics such as $V'V'_{300}$ and $V'T'_{850}$.

The present study has investigated densities of centers of migratory cyclones and anticyclones, which are influenced by both the number of tracks and their lifetime. We have compiled cyclone tracks passing the western NP domain (25°–55°N, 150°E–180°) in their lifetime. Compared to the shoulder seasons, the number of tracks increases in midwinter, which is found to dominate over the shortening of their typical lifetime and thus leading to the increase in density of NP cyclone centers as seen in Fig. 2. The result is qualitatively consistent with Schemm and Schneider (2018), and at least not contradicting the results for cyclones identified with 850-hPa vorticity by Hadas and Kaspi (2021), in the sense that the reduction in their lifetime is more distinct than that in their number. Note that their results are based on an aquaplanet GCM experiment with no land–sea contrasts, unlike around the JPS domain. Interestingly, the midwinter decrease in the number of anticyclone tracks is also found to contribute to the MWM of the density of NP anticyclone centers on top of the shortening of their typical lifetime. Another aspect possibly relevant to this study is that typical lifetime of cyclone tracks passing the JPS domain is not clearly reduced in midwinter, while that of the corresponding anticyclones exhibits a distinct MWM. This may be interpreted as the different characteristics of vertical coupling between upper- and lower-tropospheric eddies for cyclones and anticyclones over the midwinter JPS. Specifically, surface cyclones are more likely to be coupled with

upper-level cyclonic vortices with the locally lowered tropopause under the moderate background westerly wind speed on the poleward flank of the jet axis after their northeastward propagation into the NP (Fig. 1). By contrast, migratory anticyclones are less likely to form, because the frequency of upper-level anticyclonic vortices is climatologically reduced, and excessively strong background westerlies hamper the vertical coupling around the jet axis (Nakamura and Sampe 2002), owing to their southeastward propagation.

The composite analysis associated with JPS migratory anticyclones suggests their close relation to the EU teleconnection pattern. It has been suggested that the EU pattern exerts an influence onto the activity of the East Asian winter monsoon (Wang and Zhang 2015; Takaya and Nakamura 2013). The strength of the East Asian winter monsoon and upper-level East Asian trough is also closely related to the western Pacific (WP)-like pattern (Takaya and Nakamura 2013; Wang and Chen 2014; Song et al. 2016). Compared to those previous studies, the anomalous low-frequency circulation typically associated with a JPS anticyclone is characterized more by Rossby wave propagation over Eurasia rather than a WP-like anomaly (Fig. 9). It has been suggested that the EU pattern is linked more to North Atlantic SST anomalies, while the WP pattern tends to be under the remote influences of the ENSO variability (Takaya and Nakamura 2013) and the variability of the Australian summer monsoon (Sekizawa et al. 2021). Additionally, it may be for a future topic to investigate the possible influence of Arctic sea ice, especially over the Barents–Kara Sea, on the long-term modulations of the MWM through the modulated strength of the East Asian winter monsoon (Mori et al. 2014, 2019; Zhang et al. 2018) is to be investigated.

The results shown in this study are based on a single tracking algorithm that focuses on temporarily unfiltered SLP. Statistics regarding feature tracking are rather sensitive to the tracking algorithm, the parameter being tracked, as well as whether any filtering has been applied in advance (Neu et al. 2013). Although the winter-mean climatological densities of cyclones and anticyclones are compatible with previous studies (see appendix), the results in this study may be sensitive to the choice of algorithms and fields to which they are applied, especially regarding the seasonality and the relationship between anticyclones around the JPS domain and low-frequency weakening of the East Asian trough. A temporal filtering, especially with a cutoff period of about a week or 10 days, tends to overemphasize wavelike characteristics of eddies and potentially leads to the emergence of eddy centers that are not identified in the original field (not shown). To avoid such effect of filtering, this study utilizes unfiltered total SLP for tracking cyclones/anticyclones. Nevertheless, Donohoe and Battisti (2009) and Chang (2014) showed that results of cyclone tracking, especially their amplitude, change when cyclones are identified as perturbations about low-frequency background, which warrants further investigations.

Considering that the midwinter suppression of storm-track activity is a unique phenomenon for the NP, comparison of the seasonality in cyclone and anticyclone densities between the NP and NA storm tracks is also needed. In fact, our preliminary result indicates that the seasonality in cyclonic and anticyclonic densities over the NA is not as discernible as over the NP (not shown). The brief investigation of the long-term modulations of the MWM of the NP storm-track activity in this study should be complemented by a more detailed study in future. Interannual variability of the storm-track activity is also to be examined.

Acknowledgments. The authors are grateful to the three anonymous reviewers for their sound criticism and constructive comments on the earlier versions of this paper. This study is supported in part by the Japanese Ministry of Education, Culture, Sports, Science and Technology (MEXT) through the Arctic Challenge for Sustainability (ArCS-II) and through the advanced studies of climate change projection (SENTAN) Grant JPMXD0722680395, by the Japan Science and Technology Agency through COI-NEXT JPMJPF2013, by the Environmental Restoration and Conservation Agency of Japan through Environment Research and Technology Development Fund JPMEERF20222002, and by the Japan Society for the Promotion of Science (JSPS) through Grants-in-Aid for Scientific Research 19H05702 (on Innovative Areas 6102), 20H01970, 22H01292, and 22K14097. It is also supported by JSPS–ISF Joint Research Project (JPJSBP120218403). Y.K. acknowledges support from the JSPS Invitational Fellowship for Research in Japan that supported a sabbatical at The University of Tokyo and ignited this collaboration, for support from the Research Center for Advanced Technology and Science at the University of Tokyo and the Israeli Science Foundation (Grant 996/20).

Data availability statement. The JRA-55 atmospheric dataset is available online from the Japan Meteorological Agency at https://jra.kishou.go.jp/JRA-55/index_en.html as cited in Kobayashi et al. (2015) and Harada et al. (2016). The d4PDF is available at http://www.miroc-gcm.jp/~pub/d4PDF/index_en.html.

APPENDIX

Assessment of Feature Tracking Algorithm

In this study, tracks of surface centers of migratory cyclones and anticyclones are objectively identified by the procedure described in section 2. It is established that identification of cyclone tracks can be influenced by a tracking scheme used (Ulbrich et al. 2009). Therefore, given the identification algorithm used in this study includes some degree of arbitrariness, it is important to assess the performance of the tracking algorithm.

As the most intuitive way, we have verified identified cyclone and anticyclone centers in snapshots. As mentioned in section 2, the procedure has been constructed to identify features as migratory synoptic-scale cyclones and anticyclones represented on a surface weather map. Indeed, identified centers are consistent with an SLP field as a given snapshot in Fig. A1a.

It is also of particular importance to compare our tracking results with those in previous studies. The wintertime (DJF)

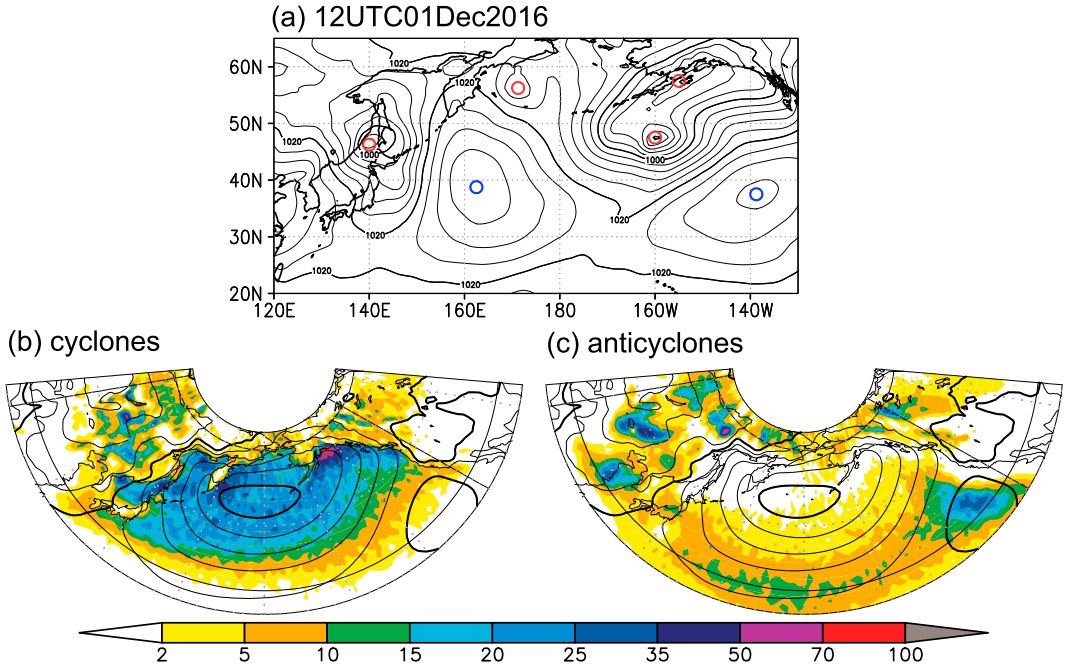

FIG. A1. (a) Snapshot of SLP (black contours; every 4 hPa) and identified cyclone and anticyclone centers (red and blue open circles, respectively) at 1200 UTC 1 Dec 2016. (b) Wintertime (DJF) climatological-mean density of identified surface cyclone centers [% $(1000\ \text{km})^{-2}$] based on the JRA-55 for the period 1958/59–2016/17. Unit is set to be the same in Neu et al. (2013). Meridians of 100°E and 120°W are highlighted, which indicate the western and eastern boundaries of the domain through which the identified centers must pass. (c) As in (b), but for identified anticyclone centers.

cyclone density with our tracking algorithm is clearly within a range of variations among those algorithms in the IMILAST project (Neu et al. 2013) in its overall density values and horizontal distribution. It is noteworthy that the cyclone density with our algorithm is consistent especially with that with algorithms using both SLP and ∇^2SLP (or, equivalently, surface vorticity). Meanwhile, the anticyclonic density has much fewer articles/literature to be compared with. Nevertheless, our result is qualitatively consistent with the results by Hoskins and Hodges (2002) and Pepler et al. (2019). One discernible characteristic of our result compared with the previous studies, especially Hoskins and Hodges (2002), is a density maximum over the eastern NP collocated with the climatological center of the southeastward-retreated wintertime subtropical high. The difference is presumably caused by the different ways of calculating density from track data to draw spatial maps. That is, while Hoskins and Hodges (2002) computed density using all grid points along a given track, the present study assembles grid points at which an anticyclone center exists in a particular time step. The difference should lead to lower (higher) density over domains where a typical propagation speed of anticyclones is fast (slow) compared to Hoskins and Hodges (2002), which can be evidently seen in Fig. A1c. We confirm that the density maximum over the eastern NP becomes less distinct when all grid points along a track are taken into account (not shown). Nevertheless, the density of centers of features is comparable more directly with results for Eulerian eddy statistics (Okajima et al. 2022).

REFERENCES

Afargan, H., and Y. Kaspi, 2017: A midwinter minimum in North Atlantic storm track intensity in years of a strong jet. *Geophys. Res. Lett.*, **44**, 12 511–12 518, https://doi.org/10.1002/2017GL075136.

Archer, C. L., and K. Caldeira, 2008: Historical trends in the jet streams. *Geophys. Res. Lett.*, **35**, L08803, https://doi.org/10.1029/2008GL033614.

Battalio, J. M., 2022: Transient eddy kinetic energetics on Mars in three reanalysis datasets. *J. Atmos. Sci.*, **79**, 361–382, https://doi.org/10.1175/JAS-D-21-0038.1.

Bell, G. D., and L. F. Bosart, 1989: A 15-year climatology of Northern Hemisphere 500 mb closed cyclone and anticyclone centers. *Mon. Wea. Rev.*, **117**, 2142–2164, https://doi.org/10.1175/1520-0493(1989)117<2142:AYCONH>2.0.CO;2.

Blackmon, M. L., 1976: A climatological spectral study of the 500 mb geopotential height of the Northern Hemisphere. *J. Atmos. Sci.*, **33**, 1607–1623, https://doi.org/10.1175/1520-0469(1976)033<1607:ACSSOT>2.0.CO;2.

——, J. M. Wallace, N. C. Lau, and S. L. Mullen, 1977: An observational study of the Northern Hemisphere wintertime circulation. *J. Atmos. Sci.*, **34**, 1040–1053, https://doi.org/10.1175/1520-0469(1977)034<1040:AOSOTN>2.0.CO;2.

——, Y. H. Lee, and J. M. Wallace, 1984: Horizontal structure of 500 mb height fluctuations with long, intermediate and short time scales. *J. Atmos. Sci.*, **41**, 961–980, https://doi.org/10.1175/1520-0469(1984)041<0961:HSOMHF>2.0.CO;2.

Bueh, C., and H. Nakamura, 2007: Scandinavian pattern and its climatic impact. *Quart. J. Roy. Meteor. Soc.*, **133**, 2117–2131, https://doi.org/10.1002/qj.173.

Catto, J. L., L. C. Shaffrey, and K. I. Hodges, 2010: Can climate models capture the structure of extratropical cyclones? *J. Climate*, **23**, 1621–1635, https://doi.org/10.1175/2009JCLI3318.1.

Chang, E. K., 2001: GCM and observational diagnoses of the seasonal and interannual variations of the Pacific storm track during the cool season. *J. Atmos. Sci.*, **58**, 1784–1800, https://doi.org/10.1175/1520-0469(2001)058<1784:GAODOT>2.0.CO;2.

——, 2005: The impact of wave packets propagating across Asia on Pacific cyclone development. *Mon. Wea. Rev.*, **133**, 1998–2015, https://doi.org/10.1175/MWR2953.1.

——, 2014: Impacts of background field removal on CMIP5 projected changes in Pacific winter cyclone activity. *J. Geophys. Res. Atmos.*, **119**, 4626–4639, https://doi.org/10.1002/2013JD020746.

——, and S. Song, 2006: The seasonal cycles in the distribution of precipitation around cyclones in the western North Pacific and Atlantic. *J. Atmos. Sci.*, **63**, 815–839, https://doi.org/10.1175/JAS3661.1.

——, and P. Zurita-Gotor, 2007: Simulating the seasonal cycle of the Northern Hemisphere storm tracks using idealized nonlinear storm-track models. *J. Atmos. Sci.*, **64**, 2309–2331, https://doi.org/10.1175/JAS3957.1.

——, and Y. Guo, 2012: Is Pacific storm-track activity correlated with the strength of upstream wave seeding? *J. Climate*, **25**, 5768–5776, https://doi.org/10.1175/JCLI-D-11-00555.1.

——, S. Lee, and K. L. Swanson, 2002: Storm track dynamics. *J. Climate*, **15**, 2163–2183, https://doi.org/10.1175/1520-0442(2002)015<02163:STD>2.0.CO;2.

Christoph, M., U. Ulbrich, and P. Speth, 1997: Midwinter suppression of Northern Hemisphere storm track activity in the real atmosphere and in GCM experiments. *J. Atmos. Sci.*, **54**, 1589–1599, https://doi.org/10.1175/1520-0469(1997)054<1589:MSONHS>2.0.CO;2.

Deng, Y., and M. Mak, 2005: An idealized model study relevant to the dynamics of the midwinter minimum of the Pacific storm track. *J. Atmos. Sci.*, **62**, 1209–1225, https://doi.org/10.1175/JAS3400.1.

Donohoe, A., and D. S. Battisti, 2009: The amplitude asymmetry between synoptic cyclones and anticyclones: Implications for filtering methods in feature tracking. *Mon. Wea. Rev.*, **137**, 3874–3887, https://doi.org/10.1175/2009MWR2837.1.

Eady, E. T., 1949: Long waves and cyclone waves. *Tellus*, **1** (3), 33–52, https://doi.org/10.3402/tellusa.v1i3.8507.

Favre, A., and A. Gershunov, 2006: Extra-tropical cyclonic/anticyclonic activity in north-eastern Pacific and air temperature extremes in western North America. *Climate Dyn.*, **26**, 617–629, https://doi.org/10.1007/s00382-005-0101-9.

Frierson, D. M. W., and N. A. Davis, 2011: The seasonal cycle of midlatitude static stability over land and ocean in global reanalyses. *Geophys. Res. Lett.*, **38**, L13803, https://doi.org/10.1029/2011GL047747.

Hadas, O., and Y. Kaspi, 2021: Suppression of baroclinic eddies by strong jets. *J. Atmos. Sci.*, **78**, 2445–2457, https://doi.org/10.1175/JAS-D-20-0289.1.

Harada, Y., and Coauthors, 2016: The JRA-55 reanalysis: Representation of atmospheric circulation and climate variability. *J. Meteor. Soc. Japan*, **94**, 269–302, https://doi.org/10.2151/jmsj.2016-015.

Harnik, N., and E. K. Chang, 2004: The effects of variations in jet width on the growth of baroclinic waves: Implications for midwinter Pacific storm track variability. *J. Atmos. Sci.*, **61**, 23–40, https://doi.org/10.1175/1520-0469(2004)061<0023:TEOVIJ>2.0.CO;2.

Held, I. M., 1978: The vertical scale of an unstable baroclinic wave and its importance for eddy heat flux parameterizations. *J. Atmos. Sci.*, **35**, 572–576, https://doi.org/10.1175/1520-0469(1978)035<0572:TVSOAU>2.0.CO;2.

Hewson, T. D., and H. A. Titley, 2010: Objective identification, typing and tracking of the complete life-cycles of cyclonic features at high spatial resolution. *Meteor. Appl.*, **17**, 355–381, https://doi.org/10.1002/met.204.

Hinman, R., 1888: *Eclectic Physical Geography*. American Book Company, 382 pp.

Hodges, K. I., 1994: A general method for tracking analysis and its application to meteorological data. *Mon. Wea. Rev.*, **122**, 2573–2586, https://doi.org/10.1175/1520-0493(1994)122<2573:AGMFTA>2.0.CO;2.

——, 1995: Feature tracking on the unit sphere. *Mon. Wea. Rev.*, **123**, 3458–3465, https://doi.org/10.1175/1520-0493(1995)123<3458:FTOTUS>2.0.CO;2.

Hoskins, B. J., and K. I. Hodges, 2002: New perspectives on the Northern Hemisphere winter storm tracks. *J. Atmos. Sci.*, **59**, 1041–1061, https://doi.org/10.1175/1520-0469(2002)059<1041:NPOTNH>2.0.CO;2.

——, and ——, 2019a: The annual cycle of Northern Hemisphere storm tracks. Part I: Seasons. *J. Climate*, **32**, 1743–1760, https://doi.org/10.1175/JCLI-D-17-0870.1.

——, and ——, 2019b: The annual cycle of Northern Hemisphere storm tracks. Part II: Regional detail. *J. Climate*, **32**, 1761–1775, https://doi.org/10.1175/JCLI-D-17-0871.1.

Ioannidou, L., and M. K. Yau, 2008: A climatology of the Northern Hemisphere winter anticyclones. *J. Geophys. Res.*, **113**, D08119, https://doi.org/10.1029/2007JD008409.

James, I. N., 1987: Suppression of baroclinic instability in horizontally sheared flows. *J. Atmos. Sci.*, **44**, 3710–3720, https://doi.org/10.1175/1520-0469(1987)044<3710:SOBIIH>2.0.CO;2.

Klein, W. H., 1958: The frequency of cyclones and anticyclones in relation to the mean circulation. *J. Meteor.*, **15**, 98–102, https://doi.org/10.1175/1520-0469(1958)015<0098:TFOCAA>2.0.CO;2.

Kobayashi, C., H. Endo, Y. Ota, S. Kobayashi, H. Onoda, Y. Harada, K. Onogi, and H. Kamahori, 2014: Preliminary results of the JRA-55C, an atmospheric reanalysis assimilating conventional observations only. *SOLA*, **10**, 78–82, https://doi.org/10.2151/sola.2014-016.

Kobayashi, S., and Coauthors, 2015: The JRA-55 reanalysis: General specifications and basic characteristics. *J. Meteor. Soc. Japan*, **93**, 5–48, https://doi.org/10.2151/jmsj.2015-001.

Kravtsov, S., I. Rudeva, and S. K. Gulev, 2015: Reconstructing sea level pressure variability via a feature tracking approach. *J. Atmos. Sci.*, **72**, 487–506, https://doi.org/10.1175/JAS-D-14-0169.1.

Kuwano-Yoshida, A., S. Okajima, and H. Nakamura, 2022: Rapid increase of explosive cyclone activity over the midwinter North Pacific in the late 1980s. *J. Climate*, **35**, 1113–1133, https://doi.org/10.1175/JCLI-D-21-0287.1.

Lachmy, O., and N. Harnik, 2014: The transition to a subtropical jet regime and its maintenance. *J. Atmos. Sci.*, **71**, 1389–1409, https://doi.org/10.1175/JAS-D-13-0125.1.

——, and ——, 2016: Wave and jet maintenance in different flow regimes. *J. Atmos. Sci.*, **73**, 2465–2484, https://doi.org/10.1175/JAS-D-15-0321.1.

Lee, S. S., J. Y. Lee, K. J. Ha, B. Wang, A. Kitoh, Y. Kajikawa, and M. Abe, 2013: Role of the Tibetan Plateau on the annual

variation of mean atmospheric circulation and storm-track activity. *J. Climate*, **26**, 5270–5286, https://doi.org/10.1175/JCLI-D-12-00213.1.

Lewis, S. R., D. P. Mulholland, P. L. Read, L. Montabone, R. J. Wilson, and M. D. Smith, 2016: The solsticial pause on Mars: 1. A planetary wave reanalysis. *Icarus*, **264**, 456–464, https://doi.org/10.1016/j.icarus.2015.08.039.

Lorenz, E. N., 1955: Available potential energy and the maintenance of the general circulation. *Tellus*, **7**, 157–167, https://doi.org/10.3402/tellusa.v7i2.8796.

Manobianco, J., 1989: Explosive east coast cyclogenesis over the west-central North Atlantic Ocean: A composite study derived from ECMWF operational analyses. *Mon. Wea. Rev.*, **117**, 2365–2383, https://doi.org/10.1175/1520-0493(1989)117<2365:EECCOT>2.0.CO;2.

Masunaga, R., H. Nakamura, B. Taguchi, and T. Miyasaka, 2020: Processes shaping the frontal-scale time-mean surface wind convergence patterns around the Kuroshio Extension in winter. *J. Climate*, **33**, 3–25, https://doi.org/10.1175/JCLI-D-19-0097.1.

Mori, M., M. Watanabe, H. Shiogama, J. Inoue, and M. Kimoto, 2014: Robust Arctic sea-ice influence on the frequent Eurasian cold winters in past decades. *Nat. Geosci.*, **7**, 869–873, https://doi.org/10.1038/ngeo2277.

——, Y. Kosaka, M. Watanabe, H. Nakamura, and M. Kimoto, 2019: A reconciled estimate of the influence of Arctic sea-ice loss on recent Eurasian cooling. *Nat. Climate Change*, **9**, 123–129, https://doi.org/10.1038/s41558-018-0379-3.

Murray, R. J., and I. Simmonds, 1991: A numerical scheme for tracking cyclone centres from digital data. *Aust. Meteor. Mag.*, **39**, 155–166.

Nakamura, H., 1992: Midwinter suppression of baroclinic wave activity in the Pacific. *J. Atmos. Sci.*, **49**, 1629–1642, https://doi.org/10.1175/1520-0469(1992)049<1629:MSOBWA>2.0.CO;2.

——, and T. Sampe, 2002: Trapping of synoptic-scale disturbances into the North-Pacific subtropical jet core in midwinter. *Geophys. Res. Lett.*, **29**, 1761, https://doi.org/10.1029/2002GL015535.

——, T. Izumi, and T. Sampe, 2002: Interannual and decadal modulations recently observed in the Pacific storm track activity and East Asian winter monsoon. *J. Climate*, **15**, 1855–1874, https://doi.org/10.1175/1520-0442(2002)015<1855:IADMRO>2.0.CO;2.

——, T. Sampe, Y. Tanimoto, and A. Shimpo, 2004: Observed associations among storm tracks, jet streams, and midlatitude oceanic fronts. *Earth's Climate: The Ocean–Atmosphere Interaction*, *Geophys. Monogr.*, Vol. 147, Amer. Geophys. Union, 329–345.

——, T. Miyasaka, Y. Kosaka, K. Takaya, and M. Honda, 2010: Northern Hemisphere extratropical tropospheric planetary waves and their low-frequency variability: Their vertical structure and interaction with transient eddies and surface thermal contrasts. *Climate Dynamics: Why Does Climate Vary*, *Geophys. Monogr.*, Vol. 189, Amer. Geophys. Union, 149–179.

Nakamura, N., 1988: Scale selection of baroclinic instability—Effects of stratification and nongeostrophy. *J. Atmos. Sci.*, **45**, 3253–3268, https://doi.org/10.1175/1520-0469(1988)045<3253:SSOBIO>2.0.CO;2.

Neu, U., and Coauthors, 2013: IMILAST: A community effort to intercompare extratropical cyclone detection and tracking algorithms. *Bull. Amer. Meteor. Soc.*, **94**, 529–547, https://doi.org/10.1175/BAMS-D-11-00154.1.

Novak, L., T. Schneider, and F. Ait-Chaalal, 2020: Midwinter suppression of storm tracks in an idealized zonally symmetric setting. *J. Atmos. Sci.*, **77**, 297–313, https://doi.org/10.1175/JAS-D-18-0353.1.

Okajima, S., H. Nakamura, and Y. Kaspi, 2021: Cyclonic and anticyclonic contributions to atmospheric energetics. *Sci. Rep.*, **11**, 13202, https://doi.org/10.1038/s41598-021-92548-7.

——, ——, and ——, 2022: Energetics of transient eddies related to the midwinter minimum of the North Pacific storm-track activity. *J. Climate*, **35**, 1137–1156, https://doi.org/10.1175/JCLI-D-21-0123.1.

Park, H. S., J. C. Chiang, and S. W. Son, 2010: The role of the central Asian mountains on the midwinter suppression of North Pacific storminess. *J. Atmos. Sci.*, **67**, 3706–3720, https://doi.org/10.1175/2010JAS3349.1.

Parker, S. S., J. T. Hawes, S. J. Colucci, and B. P. Hayden, 1989: Climatology of 500 mb cyclones and anticyclones, 1950–85. *Mon. Wea. Rev.*, **117**, 558–571, https://doi.org/10.1175/1520-0493(1989)117<0558:COMCAA>2.0.CO;2.

Penny, S., G. H. Roe, and D. S. Battisti, 2010: The source of the midwinter suppression in storminess over the North Pacific. *J. Climate*, **23**, 634–648, https://doi.org/10.1175/2009JCLI2904.1.

Pepler, A., A. Dowdy, and P. Hope, 2019: A global climatology of surface anticyclones, their variability, associated drivers and long-term trends. *Climate Dyn.*, **52**, 5397–5412, https://doi.org/10.1007/s00382-018-4451-5.

Pinto, J. G., T. Spangehl, U. Ulbrich, and P. Speth, 2005: Sensitivities of a cyclone detection and tracking algorithm: Individual tracks and climatology. *Meteor. Z.*, **14**, 823–838, https://doi.org/10.1127/0941-2948/2005/0068.

Sawyer, J. S., 1970: Observational characteristics of atmospheric fluctuations with a time scale of a month. *Quart. J. Roy. Meteor. Soc.*, **96**, 610–625, https://doi.org/10.1002/qj.49709641005.

Schemm, S., and T. Schneider, 2018: Eddy lifetime, number, and diffusivity and the suppression of eddy kinetic energy in midwinter. *J. Climate*, **31**, 5649–5665, https://doi.org/10.1175/JCLI-D-17-0644.1.

——, and G. Rivière, 2019: On the efficiency of baroclinic eddy growth and how it reduces the North Pacific storm track intensity in midwinter. *J. Climate*, **32**, 8373–8398, https://doi.org/10.1175/JCLI-D-19-0115.1.

——, H. Wernli, and H. Binder, 2021: The storm-track suppression over the western North Pacific from a cyclone life-cycle perspective. *Wea. Climate Dyn.*, **2**, 55–69, https://doi.org/10.5194/wcd-2-55-2021.

Sekizawa, S., H. Nakamura, and Y. Kosaka, 2021: Remote influence of the interannual variability of the Australian summer monsoon on wintertime climate in East Asia and the western North Pacific. *J. Climate*, **34**, 9551–9570, https://doi.org/10.1175/JCLI-D-21-0202.1.

Shaw, T. A., and Coauthors, 2016: Storm track processes and the opposing influences of climate change. *Nat. Geosci.*, **9**, 656–664, https://doi.org/10.1038/ngeo2783.

Simmonds, I., C. Burke, and K. Keay, 2008: Arctic climate change as manifest in cyclone behavior. *J. Climate*, **21**, 5777–5796, https://doi.org/10.1175/2008JCLI2366.1.

Song, L., L. Wang, W. Chen, and Y. Zhang, 2016: Intraseasonal variation of the strength of the East Asian trough and its climatic impacts in boreal winter. *J. Climate*, **29**, 2557–2577, https://doi.org/10.1175/JCLI-D-14-00834.1.

Takano, I., 2002: Analysis of an intense winter extratropical cyclone that advanced along the south coast of Japan. *J. Meteor. Soc. Japan*, **80**, 669–695, https://doi.org/10.2151/jmsj.80.669.

Takaya, K., and H. Nakamura, 2001: A formulation of a phase-independent wave-activity flux for stationary and migratory

quasigeostrophic eddies on a zonally varying basic flow. *J. Atmos. Sci.*, **58**, 608–627, https://doi.org/10.1175/1520-0469(2001)058<0608:AFOAPI>2.0.CO;2.

——, and ——, 2005: Geographical dependence of upper-level blocking formation associated with intraseasonal amplification of the Siberian high. *J. Atmos. Sci.*, **62**, 4441–4449, https://doi.org/10.1175/JAS3628.1.

——, and ——, 2013: Interannual variability of the East Asian winter monsoon and related modulations of the planetary waves. *J. Climate*, **26**, 9445–9461, https://doi.org/10.1175/JCLI-D-12-00842.1.

Takayabu, I., 1991: "Coupling development": An efficient mechanism for the development of extratropical cyclones. *J. Meteor. Soc. Japan*, **69**, 609–628, https://doi.org/10.2151/jmsj1965.69.6_609.

Tamarin, T., and Y. Kaspi, 2016: The poleward motion of extratropical cyclones from a potential vorticity tendency analysis. *J. Atmos. Sci.*, **73**, 1687–1707, https://doi.org/10.1175/JAS-D-15-0168.1.

Ulbrich, U., G. C. Leckebusch, and J. G. Pinto, 2009: Extra-tropical cyclones in the present and future climate: A review. *Theor. Appl. Climatol.*, **96**, 117–131, https://doi.org/10.1007/s00704-008-0083-8.

Wallace, J. M., and D. S. Gutzler, 1981: Teleconnections in the geopotential height field during the Northern Hemisphere winter. *Mon. Wea. Rev.*, **109**, 784–812, https://doi.org/10.1175/1520-0493(1981)109<0784:TITGHF>2.0.CO;2.

——, G. H. Lim, and M. L. Blackmon, 1988: Relationship between cyclone tracks, anticyclone tracks and baroclinic waveguides. *J. Atmos. Sci.*, **45**, 439–462, https://doi.org/10.1175/1520-0469(1988)045<0439:RBCTAT>2.0.CO;2.

Wang, C. C., and J. C. Rogers, 2001: A composite study of explosive cyclogenesis in different sectors of the North Atlantic. Part I: Cyclone structure and evolution. *Mon. Wea. Rev.*, **129**, 1481–1499, https://doi.org/10.1175/1520-0493(2001)129<1481:ACSOEC>2.0.CO;2.

Wang, L., and W. Chen, 2014: An intensity index for the East Asian winter monsoon. *J. Climate*, **27**, 2361–2374, https://doi.org/10.1175/JCLI-D-13-00086.1.

——, R. Huang, L. Gu, W. Chen, and L. Kang, 2009: Interdecadal variations of the East Asian winter monsoon and their association with quasi-stationary planetary wave activity. *J. Climate*, **22**, 4860–4872, https://doi.org/10.1175/2009JCLI2973.1.

Wang, N., and Y. Zhang, 2015: Evolution of Eurasian teleconnection pattern and its relationship to climate anomalies in China. *Climate Dyn.*, **44**, 1017–1028, https://doi.org/10.1007/s00382-014-2171-z.

Watanabe, S. I., H. Niino, and W. Yanase, 2018: Composite analysis of polar mesocyclones over the western part of the Sea of Japan. *Mon. Wea. Rev.*, **146**, 985–1004, https://doi.org/10.1175/MWR-D-17-0107.1.

Whitaker, J. S., and P. D. Sardeshmukh, 1998: A linear theory of extratropical synoptic eddy statistics. *J. Atmos. Sci.*, **55**, 237–258, https://doi.org/10.1175/1520-0469(1998)055<0237:ALTOES>2.0.CO;2.

Whittaker, L. M., and L. H. Horn, 1984: Northern Hemisphere extratropical cyclone activity for four mid-season months. *J. Climatol.*, **4**, 297–310, https://doi.org/10.1002/joc.3370040307.

Yanase, W., H. Niino, S. I. Watanabe, K. Hodges, M. Zahn, T. Spengler, and I. A. Gurvich, 2016: Climatology of polar lows over the Sea of Japan using the JRA-55 reanalysis. *J. Climate*, **29**, 419–437, https://doi.org/10.1175/JCLI-D-15-0291.1.

Yang, M., C. Li, X. Chen, Y. Tan, X. Li, C. Zhang, and G. Chen, 2021: The climatology and the midwinter suppression of the cold-season North Pacific storm track in CMIP6 models. *J. Climate*, **34**, 6971–6988, https://doi.org/10.1175/JCLI-D-20-0337.1.

Yuval, J., and Y. Kaspi, 2018: Eddy sensitivity to jet characteristics. *J. Atmos. Sci.*, **75**, 1371–1383, https://doi.org/10.1175/JAS-D-17-0139.1.

——, H. Afargan, and Y. Kaspi, 2018: The relation between the seasonal changes in jet characteristics and the Pacific midwinter minimum in eddy activity. *Geophys. Res. Lett.*, **45**, 9995–10 002, https://doi.org/10.1029/2018GL078678.

Zhang, P., Y. Wu, I. R. Simpson, K. L. Smith, X. Zhang, B. De, and P. Callaghan, 2018: A stratospheric pathway linking a colder Siberia to Barents-Kara Sea ice loss. *Sci. Adv.*, **4**, eaat6025, https://doi.org/10.1126/sciadv.aat6025.

Zhang, Y., and I. M. Held, 1999: A linear stochastic model of a GCM's midlatitude storm tracks. *J. Atmos. Sci.*, **56**, 3416–3435, https://doi.org/10.1175/1520-0469(1999)056<3416:ALSMOA>2.0.CO;2.

——, K. R. Sperber, and J. S. Boyle, 1997: Climatology and interannual variation of the East Asian winter monsoon: Results from the 1979–95 NCEP/NCAR reanalysis. *Mon. Wea. Rev.*, **125**, 2605–2619, https://doi.org/10.1175/1520-0493(1997)125<2605:CAIVOT>2.0.CO;2.

Zhao, Y., and X. S. Liang, 2019: Causes and underlying dynamic processes of the mid-winter suppression in the North Pacific storm track. *Sci. China Earth Sci.*, **62**, 872–890, https://doi.org/10.1007/s11430-018-9310-5.